Inhibition of prolyl oligopeptidase : A promising pathway to prevent the progression of age-related macular degeneration

Hellinen, Laura

2022-02

Hellinen , L , Koskela , A , Vattulainen , E , Liukkonen , M , Wegler , C , Treyer , A , Handin , N , Svensson , R , Myöhänen , T , Poso , A , Kaarniranta , K , Artursson , P & Urtti , A 2022 , ' Inhibition of prolyl oligopeptidase : A promising pathway to prevent the progression of age-related macular degeneration ' , Biomedicine & Pharmacotherapy , vol. 146 , 112501 . https://doi.org/10.1016/j.b

http://hdl.handle.net/10138/347483
https://doi.org/10.1016/j.biopha.2021.112501

Biomedicine & Pharmacotherapy 146 (2022) 112501

Contents lists available at ScienceDirect

Biomedicine & Pharmacotherapy

journal homepage: www.elsevier.com/locate/biopha

Inhibition of prolyl oligopeptidase: A promising pathway to prevent the progression of age-related macular degeneration

Laura Hellinen [a,b], Ali Koskela [c], Elina Vattulainen [c], Mikko Liukkonen [c], Christine Wegler [b,d], Andrea Treyer [b], Niklas Handin [b], Richard Svensson [d], Timo Myöhänen [a,e], Antti Poso [a], Kai Kaarniranta [c,f], Per Artursson [b,d,g], Arto Urtti [a,h,i,*]

[a] School of Pharmacy, Faculty of Health Sciences, University of Eastern Finland, 70210 Kuopio, Finland
[b] Department of Pharmacy, Uppsala University, 751 23 Uppsala, Sweden
[c] Department of Ophthalmology, Institute of Clinical Medicine, University of Eastern Finland, P.O. Box 1627, FIN-70211 , Finland
[d] Uppsala University Drug Optimization and Pharmaceutical Profiling Platform, Uppsala University, 751 23 Uppsala, Sweden
[e] Division of Pharmacology and Pharmacotherapy, Faculty of Pharmacy, University of Helsinki, Finland
[f] Department of Ophthalmology, Kuopio University Hospital, P.O. Box 1777, FIN-70211 Kuopio, Finland
[g] Science for Life Laboratory Drug Discovery and Development Platform, Uppsala University, 751 23 Uppsala, Sweden
[h] Drug Research Programme, Division of Pharmaceutical Biosciences, Faculty of Pharmacy, University of Helsinki, P.O. Box 56, FI-00014 Helsinki, Finland
[i] Laboratory of Biohybrid Technologies, Institute of Chemistry, St. Petersburg State University, Peterhoff, St. Petersburg 198504, Russia

ARTICLE INFO

Keywords:
Prolyl oligopeptidase inhibitor
Age-related macular degeneration
Autophagy
Retinal pigment epithelium
Proteomics
Target engagement

ABSTRACT

Dry age-related macular degeneration (AMD) is a currently untreatable vision threatening disease. Impaired proteasomal clearance and autophagy in the retinal pigment epithelium (RPE) and subsequent photoreceptor damage are connected with dry AMD, but detailed pathophysiology is still unclear. In this paper, we discover inhibition of cytosolic protease, prolyl oligopeptidase (PREP), as a potential pathway to treat dry AMD. We showed that PREP inhibitor exposure induced autophagy in the RPE cells, shown by increased LC3-II levels and decreased p62 levels. PREP inhibitor treatment increased total levels of autophagic vacuoles in the RPE cells. Global proteomics was used to examine the phenotype of a commonly used cell model displaying AMD characteristics, oxidative stress and altered protein metabolism, in vitro. These RPE cells displayed induced protein aggregation and clear alterations in macromolecule metabolism, confirming the relevance of the cell model. Differences in intracellular target engagement of PREP inhibitors were observed with cellular thermal shift assay (CETSA). These differences were explained by intracellular drug exposure (the unbound cellular partition coefficient, Kp_{uu}). Importantly, our data is in line with previous observations regarding the discrepancy between PREP's cleaving activity and outcomes in autophagy. This highlights the need to further explore PREP's role in autophagy so that more effective compounds can be designed to battle diseases in which autophagy induction is needed. The present work is the first report investigating the PREP pathway in the RPE and we predict that the PREP inhibitors can be further optimized for treatment of dry AMD.

1. Introduction

Increased aging of the populations will be one of the major healthcare challenges in the upcoming decades. Age-related ocular diseases burden healthcare and significantly alter the life quality of patients since vision impairment or even blindness are outcomes in some late-stage age-related ocular diseases, such as age-related macular degeneration (AMD). AMD is the most common reason for vision impairment in the industrialized countries, and the total number of AMD patients worldwide is expected to reach 288 million in 2040 [1]. AMD damages the central retina, macula, which is responsible for sharp vision, leading to loss of central vision [2]. The "wet" form of AMD is caused by neovascularization in the posterior eye segment and it can be treated with intravitreal anti-VEGF agents. However, approximately 90% of the AMD

Abbreviations: AMD, age-related macular degeneration; RPE, retinal pigment epithelium; PREP, prolyl oligopeptidase; CETSA, cellular thermal shift assay; MST, microscale thermophoresis; Kp_{uu}, unbound cellular partition coefficient; PD, Parkinson's disease; HSP, heat shock protein.

* Correspondence to: School of Pharmacy, University of Eastern Finland, POB 1627, Yliopistonranta 1 C, 70211 Kuopio, Finland.
E-mail address: arto.urtti@uef.fi (A. Urtti).

https://doi.org/10.1016/j.biopha.2021.112501
Received 5 October 2021; Received in revised form 2 December 2021; Accepted 2 December 2021
Available online 7 December 2021

patients suffer from the dry form that currently has no treatment [3]. In advanced dry AMD, geographic atrophy of the retina causes vision impairment and as with the wet form, the patients progressively lose their central vision. The dry form can eventually progress into the wet AMD. Dry AMD can be classified into early, intermediate, and late form based on the appearance of the macula [4]. In early and intermediate AMD, pigmentary changes and extracellular protein deposits are present in the macular region causing alterations in the vision. These extracellular protein deposits, 'drusen', located below the retinal pigment epithelium (RPE), are considered as the clinical hallmark for AMD [2,5,6]. In late AMD, neovascularization and/or geographic atrophy cause more severe vision impairment. The reasons behind retinal atrophy in dry AMD are not fully understood, but the vision loss is caused by RPE cell death that leads to photoreceptor damage.

The RPE functionality involves daily clearance of shed photoreceptor outer segments that leads to reactive oxygen species (ROS) formation. Therefore, the RPE cells need to endure high levels of continuous oxidative stress [7]. The RPE cells are not renewed and it has been postulated that aged cells are no longer able to protect themselves against the continuous oxidative stress leading to lipid build-up, protein aggregation and chronic inflammation which are considered to be key factors in the formation of drusens and atrophic changes in the RPE cells [8]. Even though these aspects are known to be involved in the pathophysiology of AMD, the detailed pathogenesis of the dry form is still unclear. Protein aggregation can be caused by dysfunction of several different pathways regulating the cellular protein homeostasis [9]. These include the functions of heat shock proteins (HSPs), ubiquitin-proteasome pathway and autophagy; ubiquitin-proteasome pathway being the main protein degradation pathway in eukaryotes. Both autophagy and proteasomal clearance are especially crucial for cell types with no proliferation, such as the RPE cells [10]. Dysfunctions in proteasomal clearance and autophagy are strongly connected to the etiology of AMD [11], even though the detailed pathway by which these mechanisms fail in aged cells is still unclear.

Prolyl-oligopeptidase (PREP) is a cytosolic serine protease that is involved in the degradation of small (< 30 kDa) peptides [12–14]. Inhibition of PREP has been under investigation in neurodegenerative diseases, as it has been suggested that PREP participates in the cognitive functions via maintenance of neuropeptide levels [12,13]. This led to intensive research on PREP inhibition, and several PREP inhibitors have been introduced during the 1990' s and early 2000's [14]. Most of the inhibitors are structural analogs of peptidomimetic z-proline-prolinal (ZPP, Table 1) [14,15]. The majority of the published inhibitors have been characterized by their in vitro potency (IC_{50}) towards PREP's cleaving activity, using brain extracts (e.g. bovine, porcine) or human recombinant PREP [14]. In recent years, the focus in the PREP research has however shifted from proteolytic functions of PREP to the other roles of PREP, including protein-protein interactions, cell proliferation and autophagy [16]. For example, inhibition of PREP has been shown to increase autophagy via activation of protein phosphatase 2 A (PP2A) – both in vitro and in vivo and this has led to beneficial effects in various Parkinson's disease (PD) models [17,18]. Interestingly, in protein-protein interaction related effects, the efficacy of PREP inhibitors does not correlate with proteolytic IC_{50} [19] suggesting a novel mechanism-of-action for PREP inhibitors.

Our hypothesis is that similarly as in PD models, inhibition of PREP could induce autophagy in RPE cells and thus have beneficial effects on cellular damages connected to AMD. Both diseases involve impaired autophagy and protein aggregation that cause cellular distress. Indeed, in this paper, we discover the relevance of PREP pathway in AMD by showing that PREP activity is elevated in RPE cells displaying AMD characteristics in vitro. The cell model used in our assays is based on ARPE19 cells that are exposed to proteasomal inhibitor MG-132 leading to reduced proteasomal clearance and consequently protein aggregate build-up in the cells. These cells display several characteristics relevant in AMD, such as oxidative stress and altered autophagy, shown earlier [20–22], and confirmed in this paper with pathway analysis based on global proteomics. Further, we characterized the potency and kinetics of

Table 1
PREP inhibitors.

Inhibitor	Structure	Source
2137	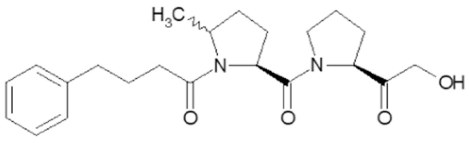	KYP compound library[33]
2153	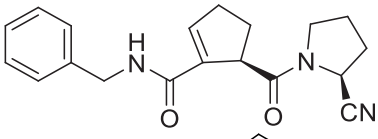	KYP compound library[33]
2189	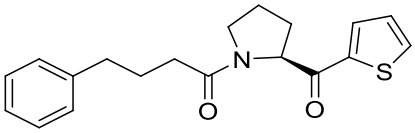	KYP compound library[34]
ZPP (Z-prolyl-prolinal)	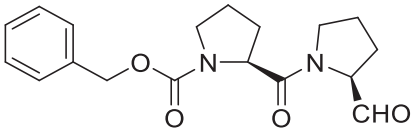	Sigma Aldrich (#SML0205); reference compound[15]
S17092	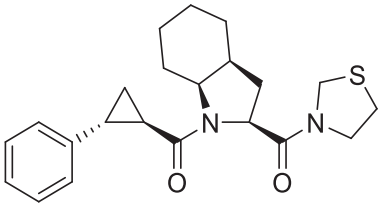	Sigma Aldrich (#SML0181); reference compound[32]

small set of PREP inhibitors. We utilized both biochemical (microscale thermophoresis, MST; IC_{50} determination) and cellular methods (cellular thermal shift assay, CETSA; unbound partition coefficient, Kp_{uu}) to verify that the compounds have desirable potency and kinetics in the RPE cells. Importantly, we demonstrate that PREP inhibitors are able to induce autophagy and prevent protein aggregation in the RPE cells. This report discovers the relevance of the PREP pathway in dry AMD and we predict that the inhibitors of PREP can be further optimized for dry AMD treatment. Fig. 1.

2. Materials and methods

2.1. Cell culture

Spontaneously arisen human RPE cell line, ARPE19, was used as the RPE cell model in this study [23]. ARPE19 cells (product of American Type Culture Collection, ATCC, #CRL-2302, Manassas, VA, USA) were maintained in DMEM-F12 medium containing 10% of fetal bovine serum (both from Gibco, Thermo Fisher Scientific, Waltham, MA, USA), 1% penicillin-streptomycin and 2 mM L-glutamine (both products of Euroclone, Pero, Italy). Passages of 15–40 were used in all assays.

The ARPE19 cells were exposed to 1 μM of proteasomal inhibitor MG-132 (#474790–5MG, Sigma-Aldrich, St. Louis, MO, USA) or to 50 nM bafilomycin (#B1793–10UG, Sigma-Aldrich, St. Louis, MO, USA) or to both of these compounds, in serum-free HBSS-Hepes (pH 7.4) or in growth medium (described above) for 24 h. Proteasomal inhibitor MG-132 was used to induce protein aggregation, whereas bafilomycin A1 was used to inhibit autophagy by preventing the formation of autolysosomes. The cells were sub-cultured at 60,000 cells/cm^2 one day prior the exposure.

HBSS-Hepes based induction was used in proteomics, CETSA and Kp_{uu} assays, whereas growth medium was utilized in activity assays and response experiments. In each assay, the control RPE cells (ARPE19) were cultured similarly than their counterparts, but the proteasomal inhibitor was not added and equal amount of vehicle (dimethyl sulfoxide, DMSO) was used instead.

2.2. PREP activity in RPE cells

Approximately 24 h after the bafilomycin and/or MG-132 treatment, the cells were collected, and PREP activity was measured. The cells were washed with phosphate buffered saline (PBS, Gibco, Thermo Fisher Scientific, Waltham, MA, USA) and homogenization buffer (50 mM KH_2PO_4, 1.5 mM $MgCl_2$, 10 mM NaCl, 1 mM EDTA, pH 7.4) was added for 5 min. The cells collected by scraping and were then incubated on ice for 20 min. The cell lysates were centrifugated (16,000 g, 10 min at + 4 °C) and the soluble fraction was collected for analysis. PREP activity was measured from supernatants using Suc-Gly-Pro-aminomethylcoumarin substrate (AMC; #4005321, Bachem, Bubendorf, Switzerland) as described earlier e.g. in Myöhänen et al., 2012 [24]. Total protein amounts were measured using the bicinchoninic acid method (BCA; Pierce BCA Protein Assay Kit, #23225, Thermo Fisher Scientific, Waltham, MA, USA), and released AMC was correlated to that.

2.3. Cell model validation with global proteomics approach

The ARPE19 cells (exposed to 1 μM MG-132 to induce protein aggregation) and normal ARPE19 cells were analyzed with global proteomics. Three normal and three MG-132 exposed ARPE19 cell samples were analyzed (passages for both were 19, 21 and 22).

2.3.1. Peptide digestion

Cell pellets with 1.4–3.4 × 10^6 cells were lysed with a 100 mM Tris-HCl buffer containing 50 mM dithiothreitol and 2% sodium dodecyl sulfate, and the tubes were heated for 5 min in boiling water followed by a sonication with a Branson-rod-type. The lysate was then centrifuged at 14,000× g for 10 min to clarify the lysate. The protein concentration was measured with tryptophan fluorescence assay [25], and 100 μg of the samples were used for multi-enzyme digestion filter-aided sample preparation (MED-FASP), where the proteins were consecutively digested with LysC and trypsin [26].

2.3.2. Peptide sample analysis

The digest were concentrated using a GeneVac EZ-2plus and injected on an Ultimate 3000 RSLCnano system coupled to a QExactive HF mass

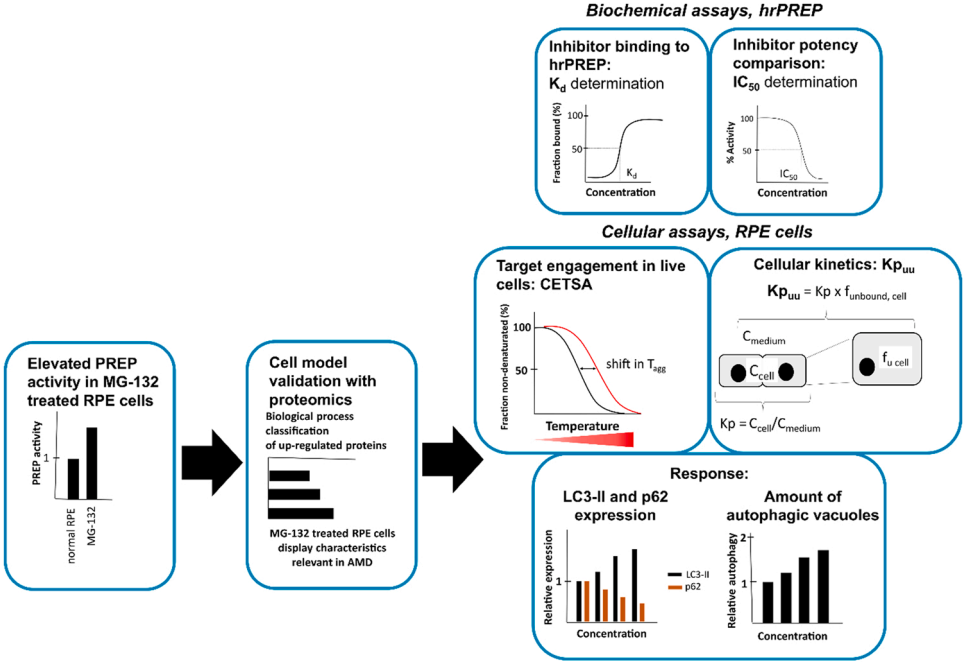

Fig. 1. Overview of the project.

spectrometer. Peptides were separated on an EASY-spray C18 reversed phase column (50 cm, 75 μm inner diameter) with a 145 min water/acetonitrile gradient containing 0.1% formic acid. Eluting peptides were subjected to a TopN = 15 method (full MS followed by ddMS^2).

2.3.3. Proteomics data analysis

MaxQuant (version 1.6.3.4) with the complete human proteome extracted from Uniprot (2018 November) was used to process the data obtained in peptide MS analysis, using the match-between-run function. The maximum false discovery rates for peptides and proteins were set to 0.01. Total protein approach was used to determine the protein expression values in fmol/μg protein [27] (Eq. 1):

$$c(i) = \frac{MS\ \ signal\ \ (i)}{Total\ \ MS\ \ signal} \times MW\ \ (i) \left[\frac{mol}{g\ \ total\ \ protein}\right] \quad (1)$$

where MS signal (i) is the sum intensities of each peptide matching the sequence of protein (i), and the total MS signal is the sum of intensities of all identified peptides. MW is the molecular weight of protein i.

The protein expression data was processed using the Perseus software [28]. The expression data of all three individually generated cell samples of both treated and untreated cells were incorporated into the data analysis. The Student's *t*-test (with permutation based FDR of 0.05) was used to determine proteins with significantly different expression values in MG-132 exposed and normal cell samples. Pathway analysis for proteins up-regulated by MG-132 treatment was performed using functional annotation clustering in DAVID (version 6.8) [29] and the PANTHER Classification system (version 14.0) [30]. In DAVID, UniProtKb keywords, GO terms for molecular function, biological process and cellular component and an EASE score of 0.5 were used for the functional annotation clustering. Enrichment scores of > 1.3 are reported (corresponding to statistically significance of $p < 0.05$). The mass spectrometry proteomics data have been deposited to the ProteomeXchange Consortium via the PRIDE [31] partner repository with the dataset identifier PXD028354.

2.4. PREP inhibitors

Two commercially available PREP inhibitors ZPP and S17092 were purchased from Sigma Aldrich (St. Louis, MO, USA). In addition, we used three molecules obtained from KYP-library (Table 1). Like majority of PREP inhibitors, including S17092 [13,14,32], KYP library compounds are peptidomimetics and structural modifications of ZPP (Table 1).

2.5. Biochemical screening methods to compare PREP inhibitor potencies

2.5.1. Determination of dissociation constants (K_d) using microscale thermophoresis (MST)

Human recombinant PREP (#80105, BPS Bioscience, San Diego, CA, USA) was labeled with Monolith His-Tag Labeling Kit RED-tris-NTA 2nd Generation (#MO-L018, NanoTemper Technologies GmbH, München, Germany) using the manufacturer's instructions. An equal volume of 200 nM hPREP in PBS-Tween (0.1%) was mixed with 100 nM RED His-Tag label (also in PBS-Tween 0.1%) and incubated at room temperature for 30 min. The labeled protein was centrifuged at 13,000 rpm for 10 min (at room temperature) and diluted into 10 nM prior the binding assay in homogenization buffer.

The binding of PREP inhibitors was determined using 7 concentrations ranging from 0.05 nM to 5000 nM. The dilutions were prepared on a PCR plate (4titude PCR Plate, Skirted, #4ti-0740, Brooks Life Sciences, Chelmsford, MA, USA) in homogenization buffer. The labeled hPREP (10 nM, V = 10 μl) was transferred into 0.2 ml PCR tubes (#I1402-8100, STARLAB GmbH, Hamburg, Germany) and an equal volume of the compound dilutions were added into the tubes. A reference sample with only labeled hPREP (c = 5 nM) in homogenization buffer was included in each assay to confirm the unbound state in the thermophoresis experiment.

After > 2 h incubation at room temperature, the hPREP–ligand complexes were centrifuged at 10,000 rpm for 5 min and transferred into the measurement capillaries (Monolith NT.115 Standard capillaries, #MO-K022, NanoTemper Technologies GmbH, München, Germany). The thermophoresis experiment was conducted with a Monolith NT.115 pico device using MO.Control Software (both from NanoTemper Technologies GmbH, München, Germany) using pico-red excitation, LED light adjusted to 60% excitation power, and MST power (infrared laser) set to high. To allow thermophoresis and fluorescence detection for 30 s, the software was used in Expert mode.

MO.Binding Affinity Software (NanoTemper Technologies GmbH, München, Germany) with the K_d binding model was used to determine the dissociation constants (K_d values). The equation is based on the Langmuir binding isotherm and it is presented below (Eq. 2; built-in analysis in the MO.Binding Affinity Software). The optimal time window to evaluate binding was selected manually by determining a region with a high signal-to-noise ratio (>5).

$$f(c) = Unbound + \frac{(Bound - Unbound) \times c + c(target) + Kd - \sqrt{(c + c(target) + Kd)^2 - 4c \times c(target)}}{2c(target)} \quad (2)$$

where f(c) is the fraction bound at a given ligand concentration c; Unbound is the normalized fluorescence (F_{norm}) at unbound state; Bound is the F_{norm} of the hPREP-ligand complex; K_d is the dissociation constant or binding affinity and c(target) is the final concentration of the target in the assay (in this case, the final concentration of hPREP was 5 nM). F_{norm} is calculated as the ratio of fluorescence at the selected time region (during thermophoresis) compared to the fluorescence at the initial phase (before heating).

2.5.2. Determination of IC_{50} values

The inhibitor potencies were determined with human recombinant PREP using commercially available PREP activity kit (BPS Biosciences). The assay was conducted on black-bottomed 96 well plates, and the formation of free AMC was monitored at one-minute intervals for 30 min. The measurements were conducted either with excitation at 360 nm and emission at 450 nm using Magellan Safire II Plate reader or with Victor Multilabel Counter with excitation 355 nm and emission 460 nm. The plate was shaken for 1 min between the measurement cycles, and the measurements were conducted at room temperature. The inhibitor concentrations were 0.005 pM-50 nM. The IC_{50} values were determined with GraphPad Prism Software (version 8.4.3), using % inhibition values at the end of the incubation time (see the details in Supplementary material).

2.6. Target engagement at cellular level (cellular thermal shift assay, CETSA)

Target engagement of the PREP inhibitors was studied with cellular thermal shift assay (CETSA) in live ARPE19 cells displaying protein aggregation (induced with 1 μM MG-132). The assay is based on ligand-

induced changes in the protein's thermal stability and the target engagement is evaluated by the observed differences in the protein's aggregation temperatures (T_{agg}) in ligand-treated and vehicle-treated treated cells [35].

2.6.1. CETSA

ARPE19 cells were seeded at 60,000 cells/cm^2. One day after the subculture, the medium was removed, and the cells were exposed to 1 μM MG-132 and the PREP inhibitors (10 μM) in HBSS-Hepes (pH 7.4). After the exposure, the cells were collected in PBS and aliquoted into 7 PCR tubes (100,000 cells/tube). The cells were pre-warmed at 37 °C for 3 min, then heated into 37, 47, 50, 53, 56, 63 or 67 °C for 3 min and subsequently cooled at 25 °C for 3 min using PCR Mastercycler (Mastercycler Pro, Eppendorf, Hamburg, Germany). After the heating, the cells were disrupted with two freeze-thaw cycles by submerging the tubes into liquid nitrogen and subsequently thawed by incubation at 25 °C for 3 min. The aggregated proteins were removed by centrifugation (at 20,000 g for 20 min at 4 °C) and the soluble fractions were diluted with Laemmli buffer (Bio-Rad, Hercules, CA, USA) and analyzed with Western blot.

2.6.2. Western blot

The proteins were separated with SDS-PAGE. Commercially available pre-cast gels (Mini-Protean TGX 4–20%) and molecular weight standard (Precision Plus Protein™ Dual Color Standard) were purchased from Bio-Rad. The proteins were transferred onto PVDF membrane with dry blotting (iBlot; Thermo Fisher Scientific, Waltham, MA, USA). The primary antibody incubation (1:1000, ab58988; Anti-Prolyl Endopeptidase antibody, Abcam, Cambridge, United Kingdom) was conducted overnight at + 4 °C. The secondary antibody incubation (1:10,000, mouse anti-rabbit IgG-HRP, Santa Cruz Biotechnology Inc, Dallas, TX, USA) took place at room temperature (for 1 h). Protein-antibody-complexes were imaged with chemiluminescence reaction (Chem-iDoc™ MP Imaging System, Bio-Rad) using Amersham™ ECL™ Prime Western Blotting Detection Reagent (GE Healthcare, Chicago, IL, USA).

2.6.3. Determination of the aggregation temperature (T_{agg})

Image Lab Software (Bio-Rad) was used to determine the intensities of the blots corresponding to the molecular weight of PREP (approximately 73 kDa in reducing conditions). The blot areas were selected with the free-hand volume tool and the band intensities (adjusted volumes) were obtained with a local background subtraction for each blot. The non-denaturated protein fractions (%) were calculated by comparing the intensities of temperature-treated cell samples to the corresponding cell samples from 37 °C.

The aggregation temperatures (T_{agg}; the temperature where 50% of the protein is in non-denaturated form) was obtained with non-linear curve fitting conducted with GraphPad Prism (version 8.4.3) using Bolzmann sigmoidal equation, as described earlier for CETSA data obtained with immunoblotting [36,37]. Thermal shift (°C) displays the difference of T_{agg} of inhibitor-treated and vehicle-treated cells.

2.7. Cellular kinetics

2.7.1. The unbound partition coefficients (Kp_{uu}) were determined as described previously [38,39]

Briefly, ARPE19 cells were sub-cultured at 60,000 cells/cm^2 on a 24 well plate. On the following day, the cells were treated with 1 μM MG-132 for 24 h in HBSS-Hepes (pH 7.4). Approximately 24 h after MG-132 treatment, the cells were exposed to 1 μM of the PREP inhibitors (2137, 2153, 2189, ZPP and S17092) and incubated for 1 h. After the incubation, the extracellular solution was collected for analysis, and the cells were rinsed rapidly twice with ice-cold PBS, followed by the intracellular compound extraction with 15 min incubation in ACN-H_2O (60:40) containing the internal standard (50 nM warfarin) at room temperature. The extracellular sample was diluted at 1:10 into ACN-H_2O (60:40) containing the internal standard (50 nM warfarin) prior the LC-MS/MS analysis. BCA protein assay (Thermo Fisher Scientific, Waltham, MA, USA) was used to determine the protein amounts in representative cell wells.

The cellular accumulation ratio (Kp) was calculated with the Eq. (3):

$$Kp = \frac{A_{cell}/V_{cell}}{c_{medium}} \quad (3)$$

Where V_{cell} is the volume of the cells (calculated with 6.5 μl/mg protein [40]), A_{cell} is the intracellular drug amount and c_{medium} is the compound concentration in the medium.

The unspecific binding to cell interior ($f_{u,\ cell}$) was determined with cell lysates in rapid equilibrium dialysis (RED) inserts. The compounds were dialyzed as a mixture, in which the concentration of each inhibitor was (0.5 μM), in cell lysates for 4 h. The $f_{u,\ homogenate}$ was determined with the Eq. (4) below:

$$f\mathrm{u},\ \mathrm{homogenate} = \frac{c_{\mathrm{buffer}}}{c_{\mathrm{homogenate}}} \quad (4)$$

Where c_{buffer} is the concentration of the compound in the buffer and the $c_{homogenate}$ is the compound concentration in the homogenate. Uniform matrix in the analysis was obtained by diluting the samples with either blank cell homogenate or HBSS-Hepes buffer.

The intracellular unbound fraction ($f_{u,cell}$) was calculated with Eq. (5):

$$f\mathrm{u},\ \mathrm{cell} = \frac{1}{D \times (1/f\mathrm{u},\ \mathrm{homogenate} - 1) + 1} \quad (5)$$

Where $f_{u,\ homogenate}$ is the unbound fraction in the homogenate (as described above) and the D is a dilution factor, calculated with the Eq. (6) below:

$$D = \frac{1000}{Protein\quad concentration\quad \left(\frac{mg}{ml}\right) \times 6.5\left(\frac{\mu g}{ml}\right)\quad protein} \quad (6)$$

In case of extremely low or no binding to cell homogenate (average $f_{u,\ homogenate}$ of 6 parallel samples > 1 and 5/6 these samples displaying $f_{u,\ homogenate} \geq 0.95$), the $f_{u,\ homogenate}$ was considered to be 1, and consequently the $f_{u,\ cell}$ was 1.

The unbound partition coefficient Kp_{uu} was obtained by multiplying the cellular accumulation ratio, Kp, with the intracellular unbound fraction, $f_{u,\ cell}$ (Eq. 7):

$$Kp\mathrm{uu} = Kp \times f\mathrm{u},\ \mathrm{cell} \quad (7)$$

2.7.2. LC-MS/MS analytics

The compound quantification was determined with liquid chromatography (Waters Acquity UPLC LC-system with either HSS T3 1.8 μm, 2.1 ×50 mm or BEH 1.7 μm, 2.1 ×50 mm column) and a triple-quadrupole mass spectrometry (QTRAP 6500, AB Sciex) using electrospray ionization. The mobile phases were formic acid (0.1%) in water (A) and acetonitrile (B). The used MS/MS conditions are described in Table 2. Warfarin was used as an internal standard in all samples.

Table 2
ESI-MS/MS conditions.

Compound	Retention time	Parent *m/z*	Declustering potential (V)	Collision energy (V)	Daughter *m/z*
2137	1.65	387.2	56	15	258.1
2153	1.57	324.2	51	27	171
2189	1.90	328.2	81	35	164
ZPP	1.62	331.2	96	23	160.2
S17092	1.93	385.3	91	33	124.1
warfarin	1.84	309.1	80	20	163

2.8. Response

2.8.1. Response (autophagy) evaluation with LC3-II and p62 protein expression

ARPE19 cells were seeded at 66,000 cells/cm^2 onto 12-well plates and incubated for 48 h to reach confluency. To study the effects of PREP inhibitors to prevent protein aggregation, the cells were treated with proteasome inhibitor MG-132 and PREP-inhibitors simultaneously. The old growth medium was replaced with a new medium containing study compounds (KYP-2137,−2153, KYP-2189, ZPP or S17092) in a range of 0.1–50 μM and MG-132 (1 μM). Control samples were treated with solvent of test compounds, DMSO, in a concentration of 25 μM. To study the ability of PREP-inhibitors to induce autophagy, the cells were first treated with the PREP-inhibitors as described above at concentration of 25 μM for 21 h. After PREP-inhibitor incubation, the lysosome inhibitor Bafilomycin 1 A (50 nM) was added to the cells to stop the autophagosome degradation and incubated for additional 3 h.

After treatments the cells were washed twice with PBS (Dulbecco's phosphate-buffered saline, Sigma-Aldrich) and 75 μl of Mammalian Protein Extraction reagent (M-PER, Thermo Scientific, Rockford, IL, USA) was added to each well for 3 min. The protein lysates were collected by scraping on ice and centrifuged at 13,000× g for 15 min at + 4 °C. The protein content of supernatants were determined using a Bradford protein assay. 20 μg of proteins were separated in 15% SDS-PAGE and transferred by wet blotting to a nitrocellulose membrane (Amersham Protran premium 0.45 μM NC, GE Healthcare, Germany). The membranes were cut above the 25 kDa band and blocked with 0.3% skim milk in Tween PBS for 1.5 h. The primary antibody for p62/SQSTM1 (Cell Signaling Technology, Danvers, MA, USA) was diluted 1:1 000 with bovine serum albumin (BSA) in 0.3% Tween PBS and incubated on the membrane over night at + 4 °C. The primary antibody for LC3 (Cell Signaling Technology) was diluted in 1:1 000 with 5% BSA in 0.1% Tween Tris-buffered saline (TBS) and added to the membranes as described above. The loading control, alpha-Tubulin (#T5168, Sigma-Aldrich, Saint Louis, MO, USA) was diluted 1:8 000 with 1% skim milk in 0.05% Tween PBS and incubated at room temperature for 15 min. After primary incubations, the secondary antibody for p62 and alpha-Tubulin, horseradish peroxidase (HRP)-linked anti-mouse (NA931, GE Healthcare), diluted 1:10,000 in 3% skim milk in 0.3% Tween PBS (for p62, 2 h) or 1% skim milk in 0.05% Tween PBS (for alpha-Tubulin, 15 min) were added on membranes. The secondary antibody for LC3, HRP-linked anti-rabbit (Novex™, #A16014, ThermoFisher Scientific, Rockford, IL, USA) was diluted 1:10,000 in 3% skim milk in 0.1 Tween TBS and added on the membranes for 2 h. All secondary antibody incubations were performed at room temperature. The bands were visualized using Immobilon Western Chemiluminescent HRP Substrate (Millipore, Billerica, MA, USA) and captured using ImageQuant RT ECL system (GE Healthcare, Little Chalfont, UK). The band quantification was performed using ImageJ software (National Institutes of Health, Bethesda, MD, USA) and the band intensities of p62 and LC3-II were normalized against alpha-Tubulin.

The immunoblotting data is presented as mean ± standard deviation (SD) (n = 3). Statistical analyses were performed using IBM SPSS statistics software version 27 (IBM, Armonk, NY, USA). The data was subjected to one-way analysis of variance (ANOVA) followed by Tukey's test for multiple comparison. P-values < 0.05 were considered significant.

2.8.2. Response evaluation with commercially available autophagy assay

We evaluated whether a commercially available Autophagy Assay Kit (#ab139484, Abcam, Cambridge, United Kingdom) could be utilized to study autophagy in the RPE cells and to detect autophagy induction caused by PREP inhibitors. According to the manufacturer, The Green Detection Dye causes minimal staining of lysosomes, but produces bright fluorescence when incorporated into pre-autophagosomes, autophagosomes and autolysosomes.

ARPE19 cells were seeded at 60,000 cells/cm^2 onto black 96 well plates with clear bottom (#10530753, Corning, NY, USA) approximately 24 h prior the compound treatment. The cells were exposed to PREP inhibitors for 24 h in serum-free growth medium (DMEM-F12 supplemented with 2 mM L-glutamine). After 24 h compound treatment, the cells were washed once with PBS and stained with Green Detection Dye (1:500 in HBSS-Hepes) for 45 min at + 37 °C. After the staining, the excess dye was removed, the cells were washed once with PBS and the fluorescence signal was measured with Hidex Sense microplate reader (Hidex, Turku, Finland) at Ex463/Em534 nm. The fluorescence values were normalized with the corresponding protein content (μg) in each cell well quantitated with the Bradford assay using Bio-Rad Protein Reagent. The level of autophagy was also evaluated in the presence of lysosomal inhibitor bafilomycin A1, and the assay was otherwise identical, but the exposure solutions were replaced to fresh ones containing bafilomycin A1 for the last 2 h of compound exposure (22–24 h). The KYP library compound 2153 was not included in these assays.

The statistical significance was evaluated with One-Way ANOVA followed by Dunnett's multiple comparisons test using GraphPad Prism Software (version version 8.4.3). P-values < 0.05 were considered significant. The number of replicates were 6–28 in different assay conditions (see the Supplementary material for details).

2.8.3. LDH release assay

ARPE19 cells were cultivated as in Section 2.8. After reaching confluency, study compounds (in a range of 15–100 μM) were added to cells in a new growth medium with or without proteasome inhibitor MG-132 (1 μM). Control cells were treated with DMSO in a concentration of 50 μM. After 24 h of exposure to the study compounds, MG-132, or DMSO, 50 μl of culture medium from each sample was added to a 96-well flat bottom microtiter plate. 50 μl of LDH assay buffer (CytoTox 96© Non-Radioactive Cytotoxicity Assay, Promega, Madison, WI, USA) was added to each sample well and mixed gently. The plate was incubated in a dark for 30 min before addition of stop solution (50 μl). Finally, the plate was gently mixed, and the absorbance was recorded at 490 nm (ELx808, BioTek Instruments, Highland Park, VT, USA). The results are shown as fold change compared to control (DMSO).

3. Results

3.1. The RPE cells treated with MG-132 display characteristics relevant to AMD in vitro

Altogether 5989 proteins were quantitated in both normal and disease-state (MG-132 exposed) ARPE19 cells (Fig. 2) – neither displayed expression of unique proteins. Out of these 5989 proteins, 149 displayed statistically significant differences in their expression levels, from which 19 proteins were down-regulated and 130 up-regulated in ARPE19 cells exposed to MG-132 (these proteins and their expression levels are presented in the Supplementary material). Pathway analysis showed that the proteins with elevated expression levels were involved, for instance, in protein ubiquitination, macromolecule metabolism, and regulation of autophagy and apoptosis (Fig. 2). The biological process classification further showed that the majority of the up-regulated proteins are involved in protein metabolism, and more specifically protein modification (Fig. 2). In addition, the MG-132 treated cells displayed up-regulation of stress-related proteins, such as HSP70 (Supplementary material). These findings confirm that the protein aggregation-induced ARPE19 cells display altered protein processing (especially proteasomal clearance due the clear up-regulation of proteins involved in ubiquitination) and suffer from oxidative stress, both known to be involved in dry AMD [11].

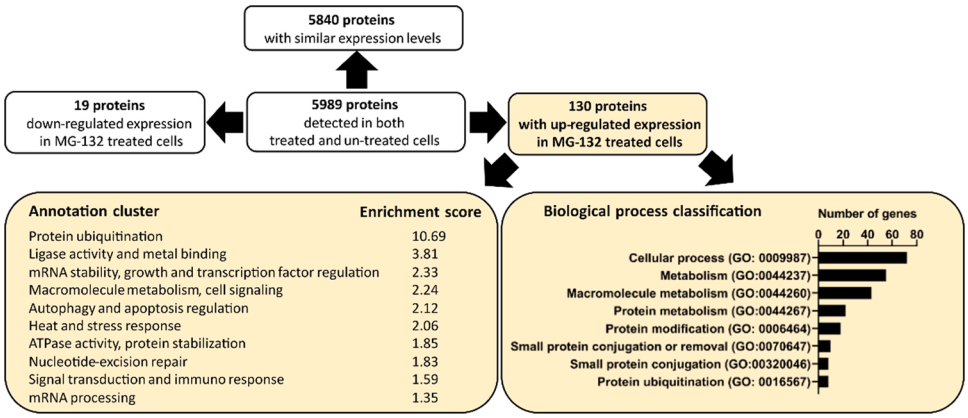

Fig. 2. Proteomics confirmed that the MG-132 induced cells display phenotype relevant in dry AMD. In total, 5989 proteins were detected in both normal and MG-132 treated cells. The 130 proteins with up-regulated expression in MG-132 treated cells are involved in, e.g., protein ubiquitination, growth factor and apoptosis regulation, and cellular stress. These pathways are relevant in dry AMD. Annotation clusters obtained with DAVID with enrichment scores > 1.3 are displayed in the image. The classification of cellular processes of up-regulated proteins in MG-132 exposed ARPE19 cells confirmed that these proteins are involved in protein metabolism and especially proteins involved in ubiquitination are up-regulated in MG-132 treated ARPE19 cells.

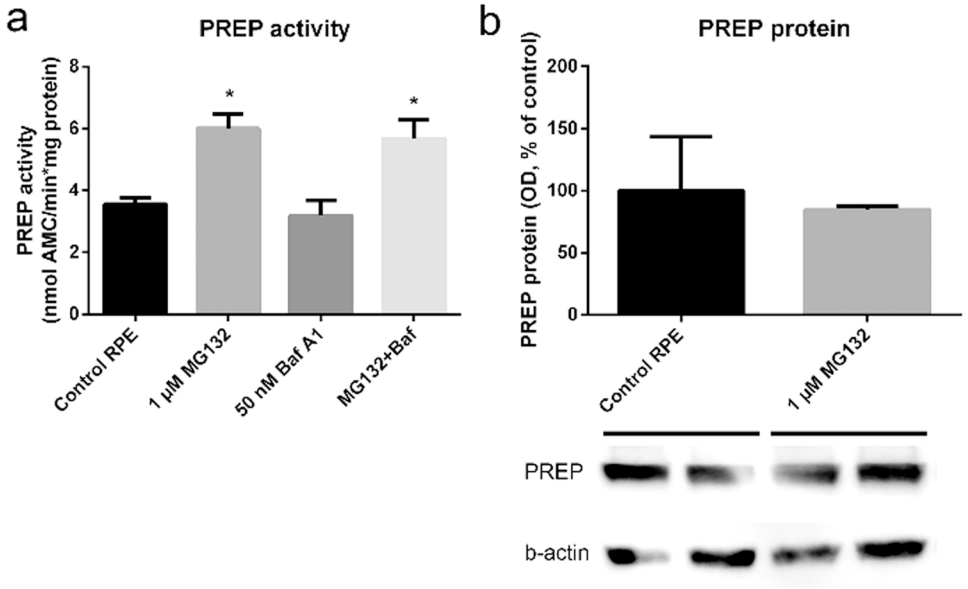

Fig. 3. PREP activity is elevated in the RPE cells treated with proteasomal inhibitor, but the protein expression is not altered. A) 24 h treatment with proteasomal inhibitor MG-132 induced PREP activity, also when co-administered with autophagy inhibitor bafilomycin A1. Bafilomycin A1 alone did not induce PREP activity ($n = 4$). The Western blot analysis of control RPE cells ($n = 2$) and MG-132 treated cells ($n = 2$) had similar PREP expression confirming that the activity induction was not caused by elevated PREP levels in MG-132 treated cells.

3.2. PREP activity, but not protein expression, is elevated in RPE cells treated with MG-132

The PREP activity increases in the presence of proteasomal inhibitor MG-132 in ARPE19 cells but not when autophagy was inhibited by bafilomycin A1 (Fig. 3A). However, the PREP protein levels were not elevated, shown with immunoblotting (Fig. 3B). Similar protein expression was verified with proteomics: the PREP expression in ARPE19 cells treated with 1 μM MG-132 was 1.96 ± 0.25 fmol/μg protein and 1.59 ± 0.17 fmol/μg protein in untreated ARPE19 cells.

Table 3
K_d and IC_{50} values of PREP inhibitors.

Compound	K_d (nM)	K_d confidence (nM)[a]	IC_{50} (nM)	IC_{50} Standard error (nM)
2137	11.7	4.9	4.7	1.5
2153	37.1	23.1	7.9	1.5
2189	36.9	8.0	11	1.6
ZPP	4.6	3.7	5.4	1.7
S17092	10.1	7.4	2.0	1.5

[a] 68% confidence values for K_d obtained within the MO. Affinity Analysis Software.

3.3. PREP inhibitors displayed affinity to and inhibition of human recombinant PREP at nanomolar concentrations

We performed both biochemical and cellular assays to assess PREP inhibition and ligand binding potency of our compound set since in the earlier studies target engagement of PREP inhibitors has been generally shown only by measuring IC_{50} of proteolytic inhibition. The K_d values and IC_{50} values were both determined with human recombinant PREP, and all the compounds displayed affinity and inhibition at nanomolar concentrations (Table 3, see the graphs in Supplementary material). Importantly, our in-house compounds had similar level of affinity and potency than the known potent PREP inhibitors (ZPP, S17092) [14] (Table 3). The rank order in the K_d values and IC_{50} values among the inhibitors was not identical. However, reasonable correlation of linear regression ($R^2 = 0.68$) was observed between these two parameters—both displaying narrow range (Fig. 4). The details regarding MST analysis (e.g. MST trace curves) are presented in the Supplementary material.

3.4. Differences in the intracellular target engagement by the PREP inhibitors was explained by cellular kinetics

CETSA was performed to further assess the target engagement of inhibitors on PREP. Clear differences in the intracellular target

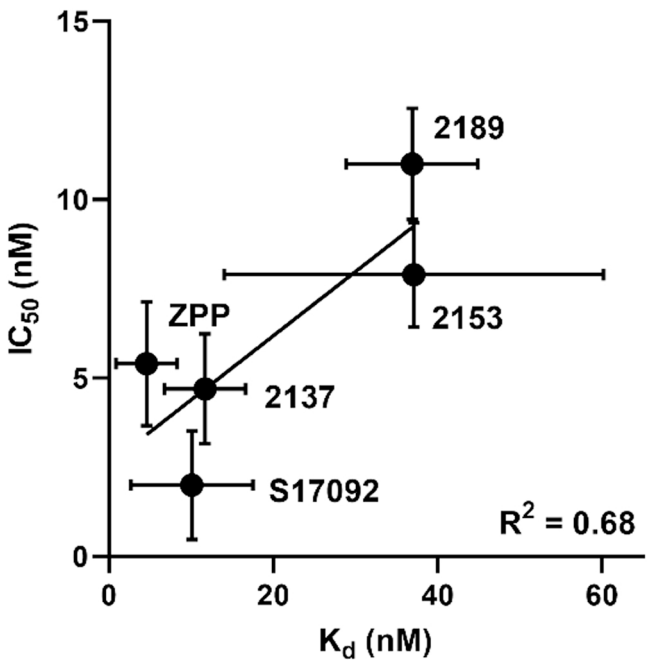

Fig. 4. The KYP **PREP inhibitor library compounds 2137, 2153 and 2189 display similar affinity and inhibition potency towards human recombinant PREP as the reference inhibitors ZPP and S17092.** The K_d values were between 4.6 and 37.1 nM and the IC_{50} values had a narrow range of 2.0–11 nM (Table 3). No major discrepancies were observed in the obtained K_d and IC_{50} values of the inhibitors (with simple linear regression $R^2 = 0.68$, generated with GraphPad Prism Software, version 8.4.3), even though the rank order was not identical. Error bars represent the 68% confidence for K_d and the standard error for IC_{50} values.

engagement by the five PREP inhibitors were seen with the CETSA. The aggregation temperature (T_{agg}) was 49.6 °C for vehicle-treated RPE cells. Significant thermal shifts were observed for cells treated with the library compounds 2137, 2135 and reference compound ZPP (Fig. 5a, b, d, f; Table 4), indicating that these compounds bound to PREP inside RPE cells. The thermal shifts for 2137 and 2153 were 4.8 and 3.2 °C, respectively. The non-linear curve fitting was unsuccessful for ZPP, i.e., T_{agg} in the presence of ZPP could not be reliably determined and therefore thermal shift of 7 °C is a rough estimate (Table 4). However, there were clear differences among the PREP protein amounts in the vehicle- and ZPP-treated cells at elevated temperatures (50, 53 and 56 °C, Fig. 5d), confirming that also ZPP bound to PREP inside RPE cells. The T_{agg} of KYP library compound 2189 and reference inhibitor S17092 were not significantly different from the vehicle results: the thermal shifts were ≤ 1 °C and the confidence intervals (CI) overlapped with the range of the vehicle data (Fig. 5c, e, f; Table 4).

The cellular kinetics explained the observed differences in the intracellular target engagement, as the KYP library compound 2189 and reference S17092 had lower intracellular exposure, as measured by Kp_{uu} (3–3.5), compared to 2137, 2153 and ZPP (7.5–10.7; Fig. 6) for which the interaction with PREP within the cellular environment was confirmed with CETSA (Fig. 5, Table 4).

3.5. PREP inhibition induces autophagy in RPE cells

We studied the pharmacological response of PREP inhibitors at the cellular level by evaluating the expression levels of p62 and LC3-II and by assessing the total amount of autophagosomal structures in RPE cells after 24 h compound treatment.

Based on p62 expression, the level of protein aggregation in RPE cells exposed to 1 μM MG-132 was more modest when the proteasomal inhibitor was co-administered with PREP inhibitors 2137, 2153, 2189 and S17092 (Fig. 7). This indicates that PREP inhibitor treatment increased the autophagic degradation and prevented the protein aggregation in RPE cells. Our library compound 2189 lacked statistical significance for p62 accumulation, however clear dose-response in the level of p62 was observed (Fig. 7c).

The levels of LC3-II were evaluated in the presence of bafilomycin A1 to stabilize autophagic flux, as bafilomycin A1 prevents the disruption of autophagosomes [41]. The expression of LC3-II clearly increased upon bafilomycin A1 treatment in the presence of PREP inhibitors 2137, 2153, 2189 and S17092 (25 μM) indicating increased formation of autophagosomes due to PREP inhibitor treatment (Fig. 8). The reference inhibitor ZPP did not have statistically significant impact on the levels of either marker protein (Figs. 7 and 8).

In addition to protein expression studies with autophagy markers LC3-II and p62, we evaluated how the level of autophagy in the RPE cells is modulated by PREP inhibitor treatment by assessing the total amount of autophagosomal structures with commercially available fluorescent dye. As serum starvation (24 h) had little effect on the observed autophagy levels in the RPE cells (Fig. 9a, inset), the relative autophagy was evaluated by comparing the cells exposed to PREP inhibitors for 24 h to untreated cells in serum-free conditions. After 24 h compound treatment, the total amount of pre-autophagosomes, autophagosomes, and autolysosomes was elevated in the RPE cells treated with PREP inhibitors 2137 (50 μM), 2189 (50 μM), and S17092 (25 and 50 μM) (Fig. 9a). Similar to the p62 and LC3-II marker studies (Figs. 7 and 8), the reference PREP inhibitor ZPP did not display statistically significant differences in autophagy levels compared to untreated control cells (Fig. 9a). These results were confirmed in the presence of bafilomycin A1—the level of autophagy in the RPE cells were higher in the cells exposed to 50 μM of our KYP library compounds 2137 and 2189 and the commercial reference S17092 (Fig. 9b), compared to cells without PREP inhibitor treatment. Bafilomycin A1 itself reduced the total fluorescence signal in the RPE cells (Fig. 9b, inset) which can be explained by the lack of autolysosome formation.

3.6. PREP inhibition did not cause toxicity in RPE cells

We examined the cellular tolerance to our library PREP inhibitors and proteasome inhibitor MG-132 with LDH leakage assay. The relative LDH leakage was similar in treated and untreated RPE cells indicating that PREP inhibitors did not cause cytotoxicity with the studied concentrations (up to 100 μM, 24 h exposure; Fig. 10). The proteasome inhibitor MG-132 expectedly increased the LDH leakage by 2-fold. However, co-treatment with PREP inhibitors did not result any further toxicity.

4. Discussion

Previous studies regarding the PREP inhibition and its potential in age-related diseases have been focusing on CNS applications, mainly to memory-related diseases and PD. In the current paper, we show that PREP activity, but not protein expression, is elevated in a cellular model that mimics AMD characteristics in vitro (Fig. 3). This suggests that similarly to neurodegenerative diseases, PREP might have an important role in age-related retinal dysfunctions. Due to this finding, we further explored a small set of PREP inhibitors in RPE cells regarding kinetics and efficacy.

Even though the detailed etiology of AMD is currently unknown, it is evident that the diseased RPE cells are unable to process cellular waste, leading to protein aggregation, inflammation and ultimately to cell death. Proteasomal clearance and autophagy are key pathways in cellular waste disposal and the loss of these functions is believed to be the major reasons behind cell distress of RPE cells in AMD [11,42,43]. Ubiquitin-proteasome system is mainly responsible for the degradation of short-lived proteins whereas autophagy can remove protein aggregates and organelles [44]. If the HSPs fail to repair proteins with

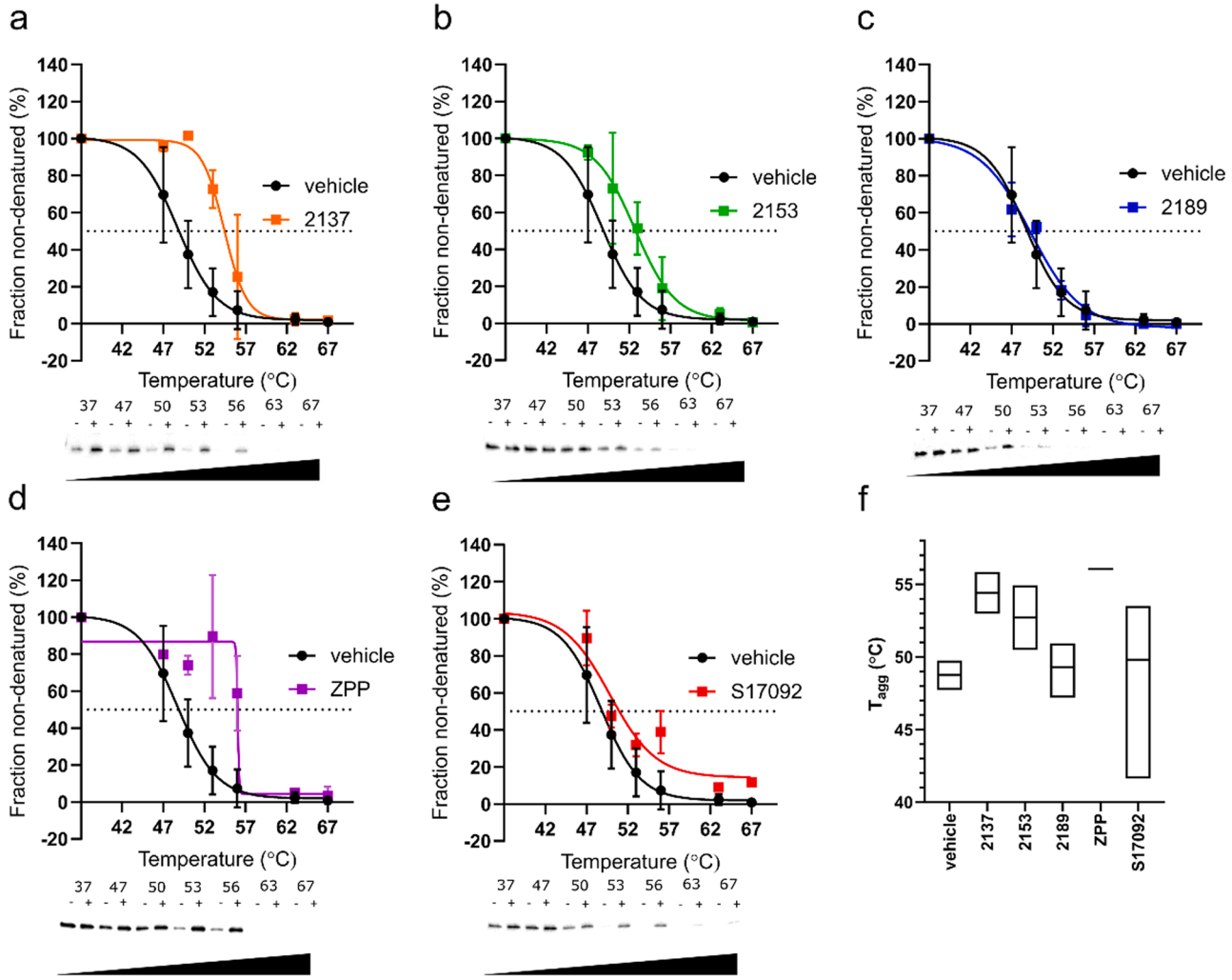

Fig. 5. Cellular thermal shift assay confirmed intracellular target engagement for KYP **compounds 2137 (a), 2153 (b) and reference compound ZPP (d), whereas thermal shift was not observed after exposure of the UEF compound 2189 (c) or reference compound S17092 (e).** The images display the average of non-denatured fractions of two individual heating cycles of treated cells and standard deviation SD. The blots are representative for both reactions. The curve fitting of vehicle controls was conducted with data from 10 individual heating cycles (the obtained data of all vehicle-treatments were combined to utilize the same vehicle control melting curve for each compound). Non-linear curve fitting (Boltzmann sigmoidal) was used to determine the temperature (T_{agg}) at which 50% of the protein (dotted line) is in its non-denatured form. f) The fitted mean aggregation temperatures (T_{agg}) and their 95% confidence intervals. Curve fitting was unsuccessful for ZPP (unable to calculate complete confidence interval, only mean estimation for T_{agg} displayed).

Table 4
CETSA parameters.

Compound	T_{agg} (°C)	95% Confidence interval (for T_{agg})	Thermal shift (°C)
vehicle	48.8	47.9–49.6	n.a.
2137	54.4	53.1–55.7	4.8
2153	52.7	50.6–54.8	3.2
2189	49.3	47.3–50.8	n.d. (< 1°C), overlapping confidence interval with the vehicle
ZPP	~56.1	fit unsuccessful	~ 7
S17092	49.8	41.8–53.4	n.d. (≤ 1 °C), overlapping confidence interval with the vehicle

n.a. not applicable, n.d. not detected.

oxidative damage, the damaged proteins are degraded by the ubiquitin-proteasome system [10]. However, damaged proteins often aggregate creating a need for autophagic degradation [45] and autophagic sequestration from the cytosol by formation of autophagosomes [46]. Eventually these vesicles fuse with lysosomes and the autophagosomal cargo is degraded by the lysosomal hydrolases. Prior to degradation by the proteasomes or autophagy, the damaged proteins are tagged via ubiquitination which involves function of several enzymes. Ubiquitination has been suggested to act as a sorting mechanism to guide proteins to be degraded by proper pathway [47].

Proteasomal inhibitor MG-132 has been used as an AMD phenotype inducer, as it has been shown to reduce proteasomal clearance [22] and cause oxidative stress [20] in the RPE, both relevant in AMD [11]. In this study, we wanted to further characterize ARPE19 cells induced to display protein aggregation with MG-132 exposure and performed global proteomics analysis of untreated and treated ARPE19 cells. Our findings confirm that the cells exposed with MG-132 represent relevant phenotype in culture, i.e., altered expression in the pathways related to macromolecule metabolism and regulation of macroautophagy and apoptosis (Fig. 2). Due the usage of proteasomal inhibitor, protein ubiquitination was clearly altered in the treated RPE cells (Fig. 2). In addition, stress markers had elevated expression levels in these cells compared to their untreated counterparts. For instance, the expression of HSP70 was induced > 10-fold in the MG-132 treated RPE cells compared to non-treated cells (Supplementary material). This indicates

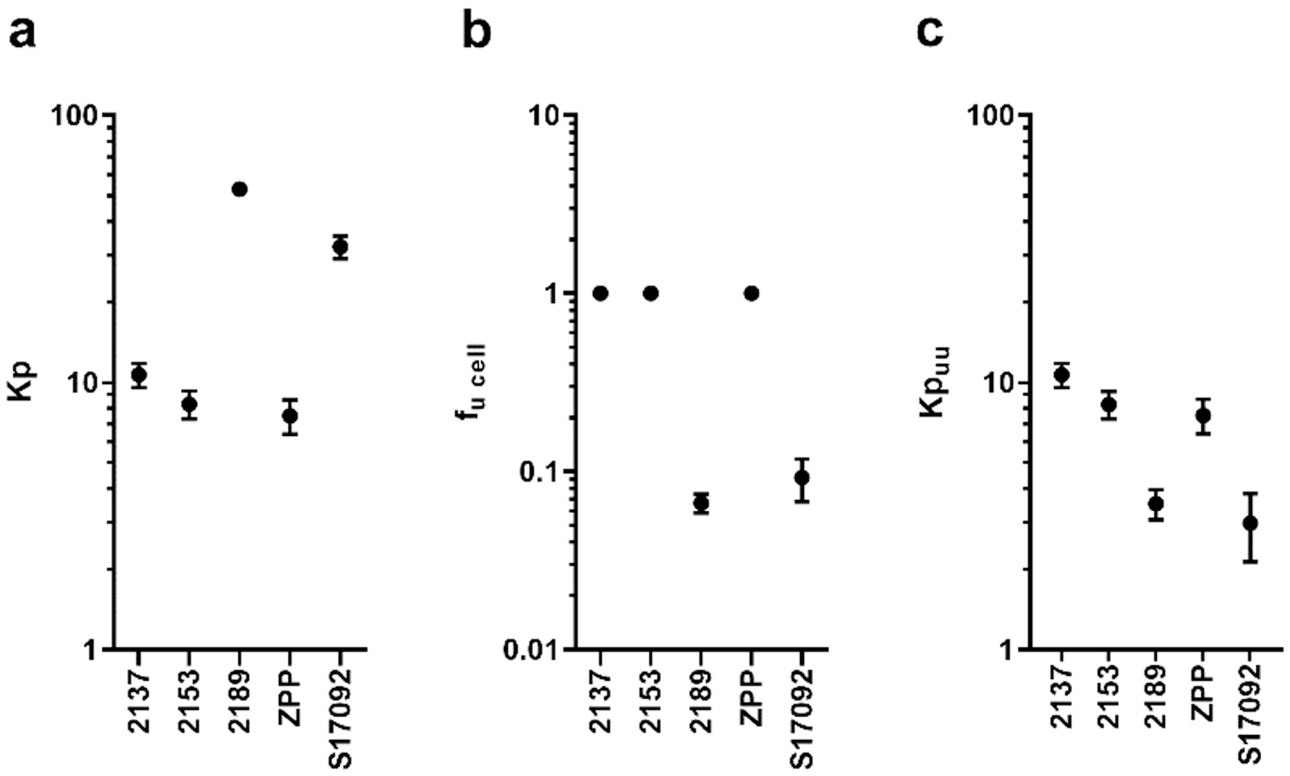

Fig. 6. Compounds with verified target engagement inside the cells (2137, 2153 and ZPP) had the highest unbound cellular accumulation ratios (Kp_{uu}). a) Cellular accumulation, Kp, was relatively high (7.5–52.9) for all studied compounds, and clearly highest for 2189 and S17092 (52.9, 32.2, respectively) **b)** Compounds 2137, 2153, and ZPP did not display unspecific binding to cell interior, whereas the free fraction (cellular unbound drug fraction, $f_{u,\ cell}$) was low for 2189 and S17092. **c)** Unbound partition coefficient (Kp_{uu}) explained the CETSA result, as the Kp_{uu} values of 2189 and S17092 were lower (3–3.5) than those observed for 2137, 2153 and ZPP (7.5–10.7).

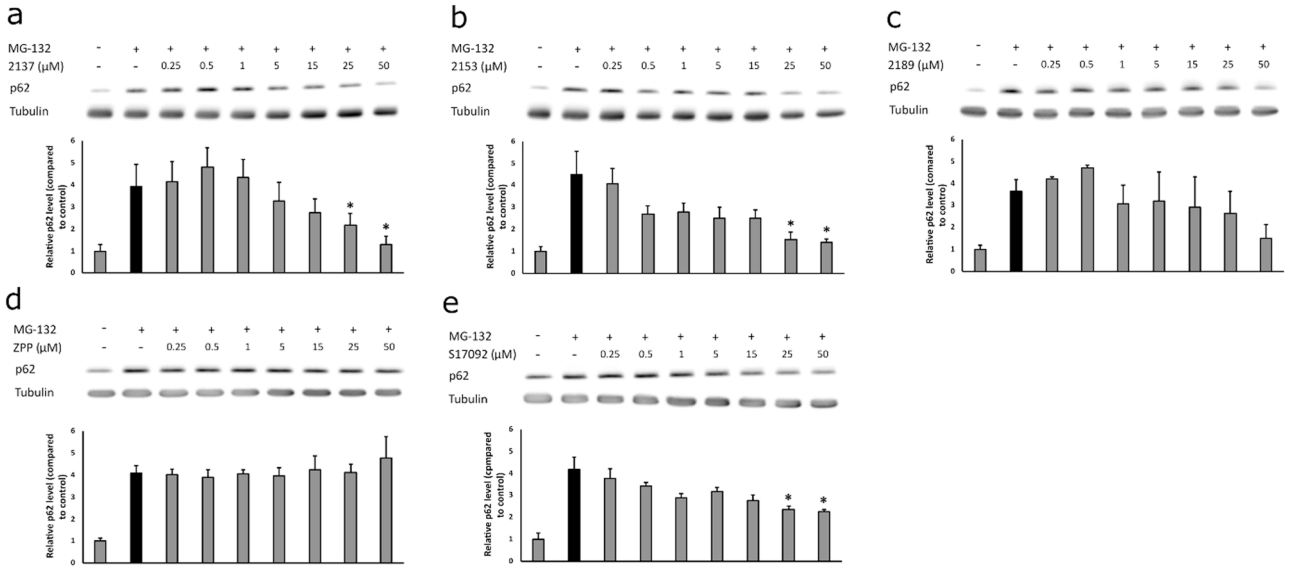

Fig. 7. PREP inhibitors a) 2137 b) 2153 and d) S17092 increase the autophagic clearance of protein aggregates upon proteasome inhibition with MG-132 (1 μM). The changes in the accumulation of p62 was used as an indicator for autophagic clearance and the statistical significance was evaluated with One-way ANOVA (*$p < 0.05$; compared to the MG-132 treated cells displayed with black bars). Neither 2189 (c) or ZPP (d) treatment resulted in statistically significant changes in the p62 levels, however, dose-response in the p62 levels is evident in case of 2189. (n = 3).

acute oxidative stress in our RPE cell model mimicking dry AMD [20]. It has been reported that HSP70 expression decreases with the severity of dry AMD [48]. Our in vitro model represents characteristics relevant to early-intermediate AMD, as the cells are not reaching atrophy. These stages are relevant in AMD drug discovery where the primary goal is to prevent the disease progression to the advanced AMD in which

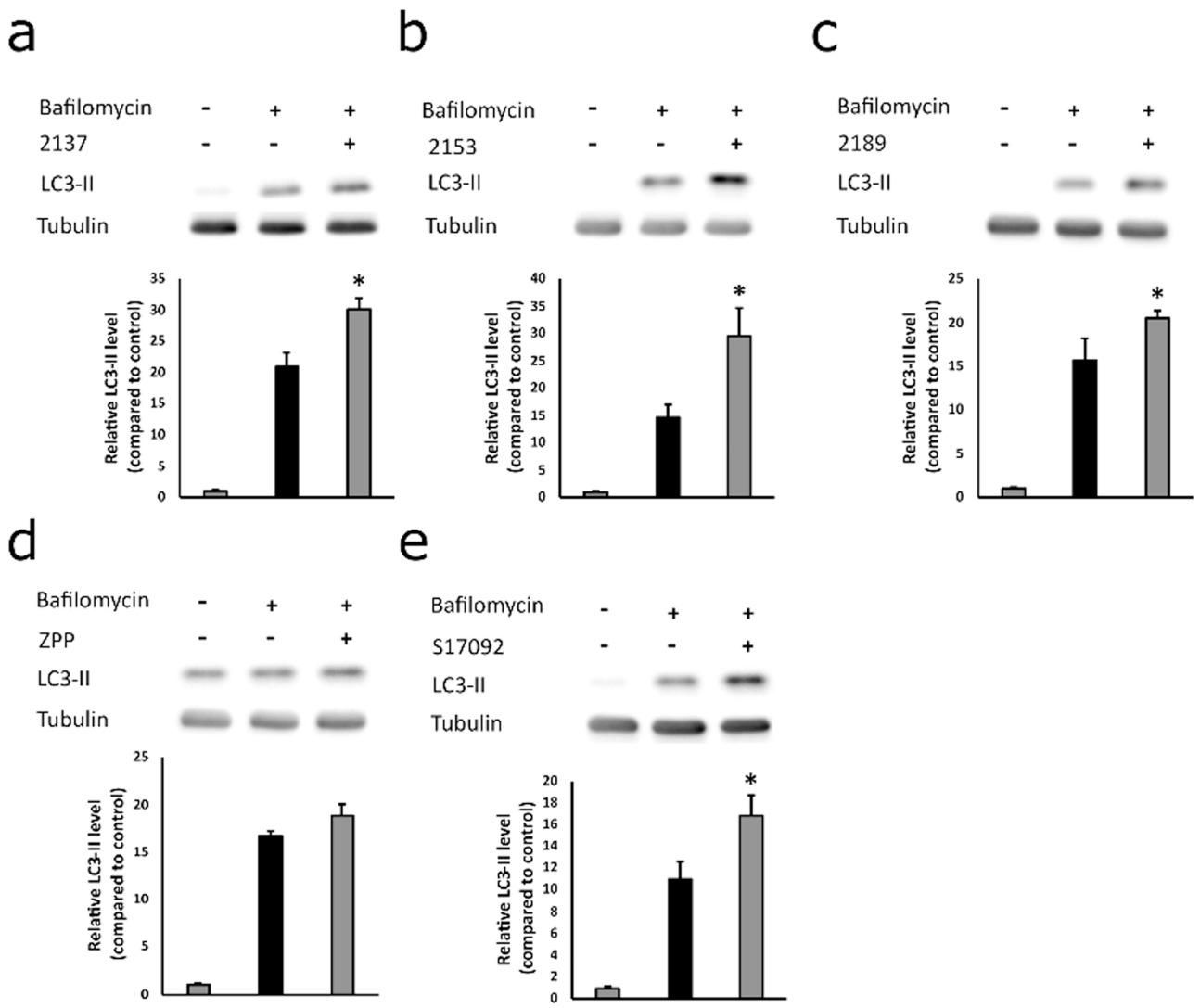

Fig. 8. The LC3-II levels were increased in the presence of PREP inhibitors 2137 (a), 2153 (b), 2189 (c) and S17092 (e) (*$p < 0.05$ One-way ANOVA; compared to the bafilomycin-treated cells displayed with black bars). The treatment with ZPP **(d)** did not result in statistically significant increase in LC3-II levels. The compounds were administered at 25 μM concentrations for 24 h, and bafilomycin A1 (50 nM) was included in the incubations during the last 3 h of the compound incubations (n = 3) to prevent the autophagosome degradation.

geographic atrophy and vision loss are seen. In late AMD where the RPE and photoreceptor cells are already lost, the treatment options would be limited to cell therapy applications, which are still experimental [49,50]. Overall, the cell model we have utilized is a useful tool in early drug discovery to study autophagy after drug exposure in RPE cells, even though the cells do not represent all features of AMD.

Autophagy is specialized to degrade aggregated proteins and cell organelles marked with p62 or ubiquitin. In this process, the p62 tagged material is first engulfed to an autophagosome via p62-LC3 interaction in a process where LC3-I is converted to a LC3-II [51]. In the second step, the autophagosome fuses with a lysosome and the material destined to autophagic clearance, along with the protein aggregation marker p62, is degraded by the lysosomal enzymes [46]. We examined the formation and degradation of protein aggregates and autophagosomes in the RPE cells by evaluating the p62 and LC3-II levels with immunoblotting and evaluated the impact PREP inhibitor treatment has for their expression. Our findings clearly show that the LC3-II levels were elevated by KYP library compounds 2137, 2153, 2189 and the commercial reference inhibitor S17092 in the presence of bafilomycin A1 that points to induced autophagy (Fig. 8). In addition, PREP inhibitors 2137, 2153 and S17092 clearly prevented the protein aggregation in the RPE cells treated with proteasomal inhibitor, evident by the lower levels of p62 after treatment with these compounds (Fig. 7). Similarly, the autophagy assay with the fluorescent dye showed that the total amount of pre-autophagosomes, autophagosomes and autolysosomes was higher after treatment with PREP inhibitors 2189, 2137 and S17092 (Fig. 9), whereas ZPP treatment did not alter the autophagy levels in the RPE cells. Taken together, these findings clearly show that treatment with PREP inhibitors can induce autophagy in RPE cells.

We compared the affinity of three in-house PREP inhibitors (2137, 2153, 2189) and two commercial reference inhibitors (ZPP, S17092) towards human recombinant PREP with MST. We showed that all studied PREP inhibitors displayed binding at nanomolar concentrations to human recombinant PREP (K_d values between 4.6 and 37 nM), and importantly, the level of binding of our library compounds was similar than the reference compounds ZPP and S17092 (Table 3). The second biochemical assay we used, the determination of IC_{50} values, is widely used to describe PREP inhibition potency [13,14]. Our data is in line with previously published IC_{50} values for inhibitors from the same molecule family (KYP library), displaying nanomolar level inhibition against porcine PREP [43–45]. Like in K_d experiments, the IC_{50} values of our inhibitors 2137, 2153, and 2189 were at similar level to the

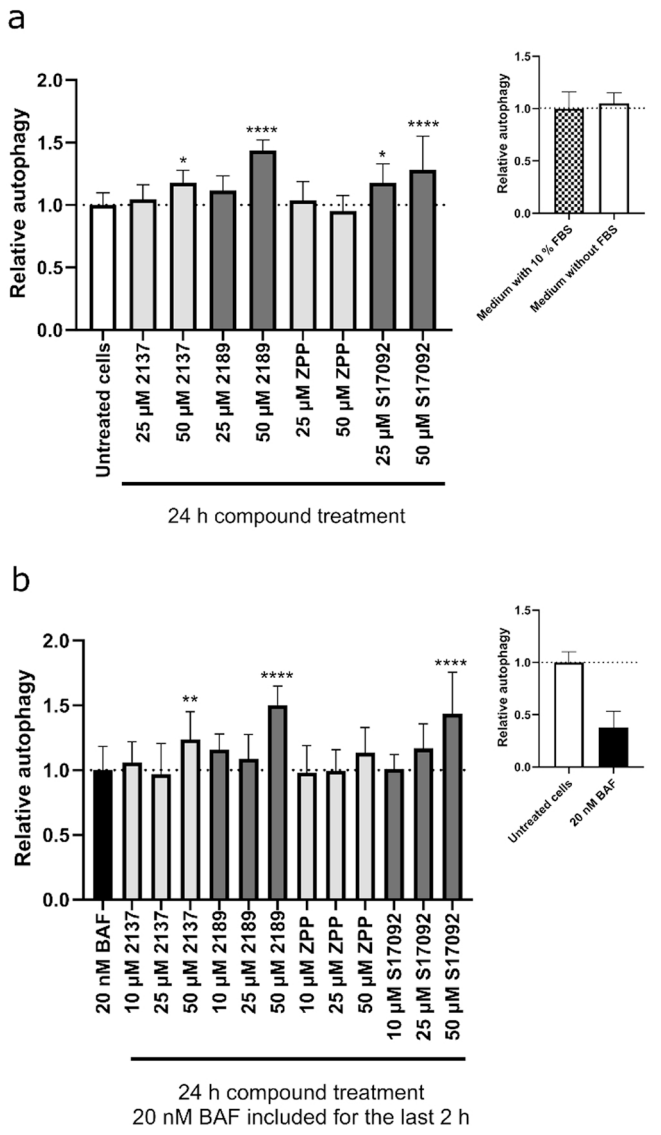

Fig. 9. PREP inhibitors 2137, 2189, and S17092 increase autophagy levels in the RPE cells. a) The RPE cells treated with 2137 (50 μM), 2189 (50 μM), and S17092 (25 and 50 μM) for 24 h had elevated autophagy levels compared to untreated RPE cells. Serum starvation had little effect on the observed autophagy levels (inset). **b)** Lysosomal inhibitor bafilomycin A1clearly reduced the observed autophagy levels in RPE cells (inset). PREP inhibitor treatment (2137, 2189 and S17092 at 50 μM) increased the autophagy also in the RPE cells co-treated with bafilomycin A1. The statistical significance was evaluated with One-way ANOVA (*$p < 0.05$, **$p < 0.01$ ****$p < 0.0001$). ZPP treatment did not result in statistically significant changes in the autophagy levels in any of the studied conditions. n = 6–28 in each condition, see the supplementary material for details.

reference compounds (Table 3) that are known to be potent PREP inhibitors [15,32]. No major discrepancies were observed between K_d and IC_{50} values (Fig. 4). However, sufficient target engagement in the cellular environment is crucial for a compound to achieve the desired therapeutic effect. Cellular thermal shift assay (CETSA) is based on ligand-induced changes in the thermal stability of proteins. When it is conducted in cellular environment, the assay enables the evaluation of binding in relevant surroundings of the endogenous protein [35]. We confirmed intracellular target engagement of ZPP and KYP library compounds 2137 and 2153 with CETSA (Table 4, Fig. 5). The biochemical screening methods were not able to predict the binding in the cellular environment, which highlights the need to assess target engagement and response in a relevant matrix. Our data of cellular binding kinetics (Kp_{uu}) explained the differences in the intracellular target engagement of the inhibitors as 2137, 2153 and ZPP displayed higher cellular unbound partition coefficient compared to 2189 and S17092 (Fig. 6). Overall, the high Kp_{uu} values of 2137, 2153 and ZPP together with the intracellular target engagement (with CETSA) indicate that the compounds can reach the cell cytoplasm and engage with PREP. In addition, we did not observe significantly higher LDH release in cells treated with our in-house PREP inhibitors compared to untreated control cells (Fig. 10). These findings are promising for further optimization and development of this molecule family for dry AMD treatment.

In earlier studies, PREP inhibitor KYP-2047 was shown to enhance the expression of beclin-1, which is an important positive regulator in the autophagosome formation [17]. Further studies showed that PREP enhances the beclin-1 mediated autophagy by acting as a negative regulator and interaction partner of protein phosphatase 2A (PP2A) complex [18]. Since this is an interaction-based regulation, enzyme conformation is more important than the block of proteolytic activity. In fact, it was shown that the inhibition against PREP's cleaving activity (IC_{50} values) does not correlate with the outcome in autophagy [19]. Our results show similar trend and in addition, there are discrepancies between the target engagement to PREP (CETSA data) and pharmacological response: ZPP had little effect on autophagy (Figs. 7–9) even though the target engagement was seen with CETSA (Fig. 5, Table 4). Similarly, ZPP did not have any effect on autophagy in HEK-293 cells [19]. Vice versa, S17092 had positive outcome on autophagy (Figs. 7–9), even though the target engagement with CETSA was not confirmed (Fig. 5, Table 4). This suggests that the impact these PREP inhibitors have on autophagy is not related to the total bound amount to the target. However no significant off-targets have been reported e.g. with KYP-2047 that is similar substrate-like PREP inhibitor as the compounds used in the current study [52]. Eventually, the effect of PREP inhibitors on autophagy is likely to be mediated via alternative binding mode or even alternative binding site in PREP, and with typical substrate-like inhibitors this appears to require higher doses than for proteolytic inhibition. This requires more detailed protein structure studies but if novel binding site in PREP can be revealed, this allows design and synthesis of completely novel PREP ligand series aimed to modify protein-protein interactions of PREP, including autophagy. Additionally, as the IC_{50} assay and CETSA seem to lack value when the autophagy induction of PREP inhibitors is evaluated, alternative approaches should be the first choice in efficacy screening. Our data demonstrated that the fluorescent autophagy dye is suitable for efficacy screening of PREP inhibitors in the RPE cells (Fig. 9), as the data was consistent with the conclusions obtained with autophagy marker expression studies (Figs. 7 and 8) and is therefore valuable tool in when larger compound libraries are screened for autophagy induction.

One possibility to further explore the pathway is to utilize thermal profiling of the cellular proteome (TPP) which couples CETSA to proteomics and is therefore a powerful tool in the field of target validation [53–55]. This approach could reveal both direct and in-direct targets of PREP inhibitors, therefore possibly revealing even other druggable targets within the pathway that would enhance autophagy and, consequently, prevent the AMD progression. TPP would be a powerful tool to evaluate specific PREP inhibitors locking the enzyme into relevant conformation. Besides the detailed characterization of the PREP pathway, further effort must be set to select not only the most potent, but also kinetically most favorable compounds to further development. The eye, and especially retina, is a kinetically challenging drug target as oral or topical ocular route generally do not provide sufficient concentrations in the posterior eye due the physiological barriers protecting these tissues [56]. The intravitreal route routinely used to treat wet AMD is not applicable for small molecules as their half-lives in vitreous are short, and weekly invasive injections are neither safe nor economical. However, with appropriate drug delivery systems, high concentrations of small molecules can be delivered to the retina over prolonged periods [56].

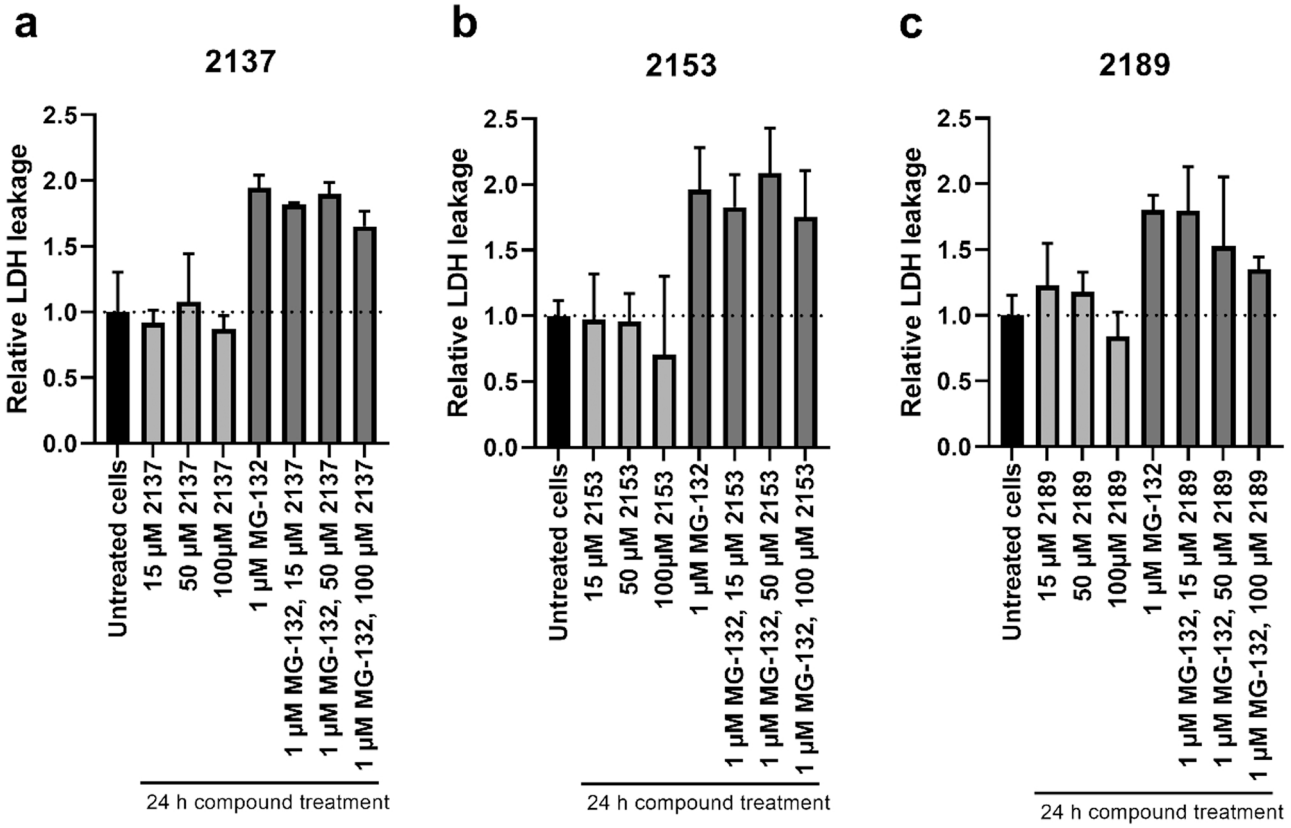

Fig. 10. PREP inhibitor treatment does not result in cytotoxicity. The PREP inhibitors **a)** 2137, **b)** 2153 or **c)** 2189 at 15–100 µM concentrations with or without 1 µM MG-132 were well tolerated by RPE cells as the LDH leakage was similar among untreated and PREP inhibitor treated cells. The images display the average of relative LDH leakage compared to the untreated cells and standard deviation SD (n = 3).

5. Conclusions

In the current paper, we demonstrated induced PREP activity in cultured RPE cells displaying characteristics relevant in AMD. We demonstrated that our own library inhibitors were as potent as the reference PREP inhibitors, all showing affinity and inhibition at nanomolar levels. Cellular binding kinetics (Kp_{uu}) was able to explain the differences of intracellular target engagement of the studied compounds that had similar potency in biochemical assays. Importantly, we showed that PREP inhibition clearly reduces protein aggregation and induces autophagy in the RPE cells. PREP inhibition is therefore an interesting pathway in AMD and should be further investigated to explore its druggability.

CRediT authorship contribution statement

Laura Hellinen Conceptualization, Methodology, Validation, Formal analysis, Investigation, Writing – original draft, Writing - Review & Editing, Visualization. **Ali Koskela** Methodology, Formal analysis, Investigation, Writing - Review & Editing, Visualization**Elina Vattulainen** Investigation. **Mikko Liukkonen** Investigation **Christine Wegrel** Methodology, Validation, Data curation, Writing - Review & Editing. **Andrea Treyer** Methodology, Validation, Data Curation, Writing - Review & Editing. **Niklas Handin** Methodology, Validation, Data Curation, Writing - Review & Editing. **Richard Svensson** Methodology, Validation, Data Curation, Writing - Review & Editing. **Timo Myöhänen** Methodology, Writing - Review & Editing, Supervision. **Antti Poso** Resources, Writing - Review & Editing, Supervision. **Kai Kaarniranta** Methodology, Resources, Writing - Review & Editing, Supervision. **Per Artursson** Methodology, Resources, Writing - Review & Editing, Supervision. **Arto Urtti** Conceptualization, Resources, Writing - Review & Editing, Supervision, Project administration, Funding acquisition.

Declaration of interests

The authors declare that they have no known competing financial interests or personal relationships that could have appeared to influence the work reported in this paper.

Acknowledgments/Funding

Academy of Finland (grant numbers 311122, 333903, 333302, 318327), Finnish Cultural Foundation (personal grant for LH), Markku Juslin grant (personal grant for LH), NordForsk (Nordic POP project 85352), and Sigrid Juselius Foundation for TM and AU. Swedish Research Council (grants no 2822 and 01951 to PA). Dr. Jukka Leppänen is acknowledged for providing NMR data.

Appendix A. Supporting information

Supplementary data associated with this article can be found in the online version at doi:10.1016/j.biopha.2021.112501.

References

[1] W.L. Wong, X. Su, X. Li, C.M. Cheung, R. Klein, C.Y. Cheng, T.Y. Wong, Global prevalence of age-related macular degeneration and disease burden projection for 2020 and 2040: a systematic review and meta-analysis, Lancet Glob. Health 2 (2014) e106–e116.

[2] K.M. Gehrs, D.H. Anderson, L.V. Johnson, G.S. Hageman, Age-related macular degeneration–emerging pathogenetic and therapeutic concepts, Ann. Med. 38 (2006) 450–471.

[3] M. La Cour, J.F. Kiilgaard, M.H. Nissen, Age-related macular degeneration: epidemiology and optimal treatment, Drugs Aging 19 (2002) 101–133.

[4] F.L. Ferris 3rd, C.P. Wilkinson, A. Bird, U. Chakravarthy, E. Chew, K. Csaky, S. R. Sadda, C. Beckman Initiative for Macular Research Classification, Clinical classification of age-related macular degeneration, Ophthalmology 120 (2013) 844–851.

[5] C. Bowes Rickman, S. Farsiu, C.A. Toth, M. Klingeborn, Dry age-related macular degeneration: mechanisms, therapeutic targets, and imaging, Investig. Ophthalmol. Vis. Sci. 54 (2013) ORSF68–ORSF80.

[6] N.G. Lambert, H. ElShelmani, M.K. Singh, F.C. Mansergh, M.A. Wride, M. Padilla, D. Keegan, R.E. Hogg, B.K. Ambati, Risk factors and biomarkers of age-related macular degeneration, Prog. Retin. Eye Res. 54 (2016) 64–102.

[7] B.S. Winkler, M.E. Boulton, J.D. Gottsch, P. Sternberg, Oxidative damage and age-related macular degeneration, Mol. Vis. 5 (1999) 32.

[8] K. Kaarniranta, D. Sinha, J. Blasiak, A. Kauppinen, Z. Veréb, A. Salminen, M. E. Boulton, G. Petrovski, Autophagy and heterophagy dysregulation leads to retinal pigment epithelium dysfunction and development of age-related macular degeneration, Autophagy 9 (2013) 973–984.

[9] C.L. Klaips, G.G. Jayaraj, F.U. Hartl, Pathways of cellular proteostasis in aging and disease, J. Cell Biol. 217 (2018) 51–63.

[10] M.S. Hipp, P. Kasturi, F.U. Hartl, The proteostasis network and its decline in ageing, Nat. Rev. Mol. Cell Biol. 20 (2019) 421–435.

[11] K. Kaarniranta, P. Tokarz, A. Koskela, J. Paterno, J. Blasiak, Autophagy regulates death of retinal pigment epithelium cells in age-related macular degeneration, Cell Biol. Toxicol. 33 (2017) 113–128.

[12] W.L. Taylor, J.E. Dixon, Catabolism of neuropeptides by a brain proline endopeptidase, Biochem. Biophys. Res. Commun. 94 (1980) 9–15.

[13] J. Lawandi, S. Gerber-Lemaire, L. Juillerat-Jeanneret, N. Moitessier, Inhibitors of prolyl oligopeptidases for the therapy of human diseases: defining diseases and inhibitors, J. Med. Chem. 53 (2010) 3423–3438.

[14] Lopez A., Tarrago T., Giralt E. Low molecular weight inhibitors of Prolyl Oligopeptidase: a review of compounds patented from 2003 to 2010. Expert Opin Ther Pat 2011; 21: 1023–1044.

[15] S. Wilk, M. Orlowski, Inhibition of rabbit brain prolyl endopeptidase by n-benzyloxycarbonyl-prolyl-prolinal, a transition state aldehyde inhibitor, J. Neurochem. 41 (1983) 69–75.

[16] R. Svarcbahs, U. Julku, T. Kilpeläinen, M. Kyyrö, M. Jäntti, T.T. Myöhänen, New tricks of prolyl oligopeptidase inhibitors – a common drug therapy for several neurodegenerative diseases, Biochem. Pharm. 161 (2019) 113–120.

[17] M.H. Savolainen, C.T. Richie, B.K. Harvey, P.T. Männistö, K.A. Maguire-Zeiss, T. T. Myöhänen, The beneficial effect of a prolyl oligopeptidase inhibitor, KYP-2047, on alpha-synuclein clearance and autophagy in A30P transgenic mouse, Neurobiol. Dis. 68 (2014) 1–15.

[18] R. Svarcbahs, M. Jäntti, T. Kilpeläinen, U.H. Julku, L. Urvas, S. Kivioja, S. Norrbacka, T.T. Myöhänen, Prolyl oligopeptidase inhibition activates autophagy via protein phosphatase 2A, Pharmacol. Res. 151 (2020), 104558.

[19] T.P. Kilpeläinen, L. Hellinen, J. Vrijdag, X. Yan, R. Svarcbahs, K.S. Vellonen, A. M. Lambeir, H. Huttunen, A. Urtti, E. Wallen, T.T. Myöhänen, The effect of prolyl oligopeptidase inhibitors on alpha-synuclein aggregation and autophagy cannot be predicted by their inhibitory efficacy, Biomed. Pharmacother. 128 (2020), 110253.

[20] T. Ryhänen, J.M. Hyttinen, J. Kopitz, K. Rilla, E. Kuusisto, E. Mannermaa, J. Viiri, C.I. Holmberg, I. Immonen, S. Meri, J. Parkkinen, E.L. Eskelinen, H. Uusitalo, A. Salminen, K. Kaarniranta, Crosstalk between Hsp70 molecular chaperone, lysosomes and proteasomes in autophagy-mediated proteolysis in human retinal pigment epithelial cells, J. Cell Mol. Med. 13 (2009) 3616–3631.

[21] J. Viiri, M. Amadio, N. Marchesi, J.M. Hyttinen, N. Kivinen, R. Sironen, K. Rilla, S. Akhtar, A. Provenzani, V.G. D'Agostino, S. Govoni, A. Pascale, H. Agostini, G. Petrovski, A. Salminen, K. Kaarniranta, Autophagy activation clears ELAVL1/HuR-mediated accumulation of SQSTM1/p62 during proteasomal inhibition in human retinal pigment epithelial cells, PLOS One 8 (2013), e69563.

[22] J. Viiri, J.M. Hyttinen, T. Ryhänen, K. Rilla, T. Paimela, E. Kuusisto, A. Siitonen, A. Urtti, A. Salminen, K. Kaarniranta, P62/sequestosome 1 as a regulator of proteasome inhibitor-induced autophagy in human retinal pigment epithelial cells, Mol. Vis. 16 (2010) 1399–1414.

[23] K.C. Dunn, A.E. Aotaki-Keen, F.R. Putkey, L.M. Hjelmeland, ARPE-19, a human retinal pigment epithelial cell line with differentiated properties, Exp. Eye Res. 62 (1996) 155–169.

[24] T.T. Myöhänen, M.J. Hannula, R. Van Elzen, M. Gerard, P. Van Der Veken, J. A. García-Horsman, V. Baekelandt, P.T. Männistö, A.M. Lambeir, A prolyl oligopeptidase inhibitor, KYP-2047, reduces alpha-synuclein protein levels and aggregates in cellular and animal models of Parkinson's disease, Br. J. Pharmacol. 166 (2012) 1097–1113.

[25] J.R. Wiśniewski, F.Z. Gaugaz, Fast and sensitive total protein and peptide assays for proteomic analysis, Anal. Chem. 87 (2015) 4110–4116.

[26] J.R. Wiśniewski, M. Mann, Consecutive proteolytic digestion in an enzyme reactor increases depth of proteomic and phosphoproteomic analysis, Anal. Chem. 84 (2012) 2631–2637.

[27] J.R. Wiśniewski, D. Rakus, Multi-enzyme digestion FASP and the 'total protein approach'-based absolute quantification of the Escherichia coli proteome, J. Proteom. 109 (2014) 322–331.

[28] S. Tyanova, T. Temu, P. Sinitcyn, A. Carlson, M.Y. Hein, T. Geiger, M. Mann, J. Cox, The Perseus computational platform for comprehensive analysis of (prote) omics data, Nat. Methods 13 (2016) 731–740.

[29] W. Huang da, B.T. Sherman, R.A. Lempicki, Systematic and integrative analysis of large gene lists using DAVID bioinformatics resources, Nat. Protoc. 4 (2009) 44–57.

[30] H. Mi, A. Muruganujan, X. Huang, D. Ebert, C. Mills, X. Guo, P.D. Thomas, Protocol Update for large-scale genome and gene function analysis with the PANTHER classification system (v.14.0), Nat. Protoc. 14 (2019) 703–721.

[31] J.A. Vizcaíno, A. Csordas, N. Del-Toro, J.A. Dianes, J. Griss, I. Lavidas, G. Mayer, Y. Perez-Riverol, F. Reisinger, T. Ternent, Q.W. Xu, R. Wang, H. Hermjakob, 2016 update of the PRIDE database and its related tools, Nucleic Acids Res. 44 (2016) 11033.

[32] H. Barelli, A. Petit, E. Hirsch, S. Wilk, G. De Nanteuil, P. Morain, F. Checler, S 17092-1, a highly potent, specific and cell permeant inhibitor of human proline endopeptidase, Biochem. Biophys. Res. Commun. 257 (1999) 657–661.

[33] Gynther J., Männistö P.T., Wallén E., Christaans H., Forsberg M., Poso A., et al. Compounds Having Prolyl Oligopeptidase Inhibitory Activity 2004.

[34] E.M. Jarho, J.I. Venäläinen, S. Poutiainen, H. Leskinen, J. Vepsäläinen, J. A. Christiaans, M.M. Forsberg, P.T. Männistö, E.A. Wallén, 2(S)-(Cycloalk-1-enecarbonyl)-1-(4-phenyl-butanoyl)pyrrolidines and 2(S)-(aroyl)-1-(4-phenylbutanoyl)pyrrolidines as prolyl oligopeptidase inhibitors, Bioorg. Med. Chem. 15 (2007) 2024–2031.

[35] D. Martinez Molina, R. Jafari, M. Ignatushchenko, T. Seki, E.A. Larsson, C. Dan, L. Sreekumar, Y. Cao, P. Nordlund, Monitoring drug target engagement in cells and tissues using the cellular thermal shift assay, Science 341 (2013) 84–87.

[36] R. Jafari, H. Almqvist, H. Axelsson, M. Ignatushchenko, T. Lundbäck, P. Nordlund, D. Martinez Molina, The cellular thermal shift assay for evaluating drug target interactions in cells, Nat. Protoc. 9 (2014) 2100–2122.

[37] M. Hashimoto, E. Girardi, R. Eichner, G. Superti-Furga, Detection of chemical engagement of solute carrier proteins by a cellular thermal shift assay, ACS Chem. Biol. 13 (2018) 1480–1486.

[38] A. Mateus, P. Matsson, P. Artursson, Rapid measurement of intracellular unbound drug concentrations, Mol. Pharm. 10 (2013) 2467–2478.

[39] A. Mateus, P. Matsson, P. Artursson, A high-throughput cell-based method to predict the unbound drug fraction in the brain, J. Med Chem. 57 (2014) 3005–3010.

[40] C.M. Gillen, B. Forbush 3rd, Functional interaction of the K-Cl cotransporter (KCC1) with the Na-K-Cl cotransporter in HEK-293 cells, Am. J. Physiol. 276 (1999) C328–C336.

[41] D.J. Klionsky, A.K. Abdel-Aziz, S. Abdelfatah, M. Abdellatif, A. Abdoli, S. Abel, H. Abeliovich, M.H. Abildgaard, Y.P. Abudu, A. Acevedo-Arozena, I. E. Adamopoulos, K. Adeli, T.E. Adolph, A. Adornetto, E. Aflaki, G. Agam, A. Agarwal, B.B. Aggarwal, M. Agnello, P. Agostinis, J.N. Agrewala, A. Agrotis, P. V. Aguilar, S.T. Ahmad, Z.M. Ahmed, U. Ahumada-Castro, S. Aits, S. Aizawa, Y. Akkoc, T. Akoumianaki, H.A. Akpinar, A.M. Al-Abd, L. Al-Akra, A. Al-Gharaibeh, M.A. Alaoui-Jamali, S. Alberti, E. Alcocer-Gómez, C. Alessandri, M. Ali, M.A. Alim Al-Bari, S. Aliwaini, J. Alizadeh, E. Almacellas, A. Almasan, A. Alonso, G.D. Alonso, N. Altan-Bonnet, D.C. Altieri, É. Álvarez, S. Alves, C. Alves da Costa, M. M. Alzaharna, M. Amadio, C. Amantini, C. Amaral, S. Ambrosio, A.O. Amer, V. Ammanathan, Z. An, S.U. Andersen, S.A. Andrabi, M. Andrade-Silva, A. M. Andres, S. Angelini, D. Ann, U.C. Anozie, M.Y. Ansari, P. Antas, A. Antebi, Z. Antón, T. Anwar, L. Apetoh, N. Apostolova, T. Araki, Y. Araki, K. Arasaki, W. L. Araújo, J. Araya, C. Arden, M.A. Arévalo, S. Arguelles, E. Arias, J. Arikkath, H. Arimoto, A.R. Ariosa, D. Armstrong-James, L. Arnauné-Pelloquin, A. Aroca, D. S. Arroyo, I. Arsov, R. Artero, D. Asaro, M. Aschner, M. Ashrafizadeh, O. Ashur-Fabian, A.G. Atanasov, A.K. Au, P. Auberger, H.W. Auner, L. Aurelian, R. Autelli, L. Avagliano, Y. Ávalos, S. Aveic, C.A. Aveleira, T. Avin-Wittenberg, Y. Aydin, S. Ayton, S. Ayyadevara, M. Azzopardi, M. Baba, J.M. Backer, S.K. Backues, D. H. Bae, O.N. Bae, S.H. Bae, E.H. Baehrecke, A. Baek, S.H. Baek, S.H. Baek, G. Bagetta, A. Bagniewska-Zadworna, H. Bai, J. Bai, X. Bai, Y. Bai, N. Bairagi, S. Baksi, T. Balbi, C.T. Baldari, W. Balduini, A. Ballabio, M. Ballester, S. Balazadeh, R. Balzan, R. Bandopadhyay, S. Banerjee, S. Banerjee, Á. Bánréti, Y. Bao, M. S. Baptista, A. Baracca, C. Barbati, A. Bargiela, D. Barilà, P.G. Barlow, S. J. Barmada, E. Barreiro, G.E. Barreto, J. Bartek, Guidelines for the use and interpretation of assays for monitoring autophagy (4th edition)(1), Autophagy 17 (2021) 1–382.

[42] J. Blasiak, E. Pawlowska, J. Szczepanska, K. Kaarniranta, Interplay between autophagy and the ubiquitin-proteasome system and its role in the pathogenesis of age-related macular degeneration, Int. J. Mol. Sci. 20 (2019) 210, https://doi.org/10.3390/ijms20010210.

[43] K. Kaarniranta, H. Uusitalo, J. Blasiak, S. Felszeghy, R. Kannan, A. Kauppinen, A. Salminen, D. Sinha, D. Ferrington, Mechanisms of mitochondrial dysfunction and their impact on age-related macular degeneration, Prog. Retin. Eye Res. 79 (2020), 100858.

[44] N.M. Kocaturk, D. Gozuacik, Crosstalk between mammalian autophagy and the ubiquitin-proteasome system, Front. Cell Dev. Biol. 6 (2018) 128.

[45] E. Lévy, N. El Banna, D. Baïlle, A. Heneman-Masurel, S. Truchet, H. Rezaei, M. E. Huang, V. Béringue, D. Martin, L. Vernis, Causative links between protein aggregation and oxidative stress: a review, Int. J. Mol. Sci. 20 (2019) 3896, https://doi.org/10.3390/ijms20163896.

[46] K.R. Parzych, D.J. Klionsky, An overview of autophagy: morphology, mechanism, and regulation, Antioxid. Redox Signal. 20 (2014) 460–473.

[47] K. Lu, F. den Brave, S. Jentsch, Pathway choice between proteasomal and autophagic degradation, Autophagy 13 (2017) 1799–1800.

[48] C.L. Nordgaard, P.P. Karunadharma, X. Feng, T.W. Olsen, D.A. Ferrington, Mitochondrial proteomics of the retinal pigment epithelium at progressive stages of age-related macular degeneration, Investig. Ophthalmol. Vis. Sci. 49 (2008) 2848–2855.

[49] H.M. Zajac-Pytrus, A. Pilecka, A. Turno-Krecicka, J. Adamiec-Mroczek, M. Misiuk-Hojlo, The dry form of age-related macular degeneration (AMD): the current

concepts of pathogenesis and prospects for treatment, Adv. Clin. Exp. Med. 24 (2015) 1099–1104.
[50] A. Kvanta, M.K. Grudzinska, Stem cell-based treatment in geographic atrophy: promises and pitfalls, Acta Ophthalmol. 92 (2014) 21–26.
[51] S. Pankiv, T.H. Clausen, T. Lamark, A. Brech, J.A. Bruun, H. Outzen, A. Øvervatn, G. Bjørkøy, T. Johansen, p62/SQSTM1 binds directly to Atg8/LC3 to facilitate degradation of ubiquitinated protein aggregates by autophagy, J. Biol. Chem. 282 (2007) 24131–24145.
[52] A.J. Jalkanen, T.P. Piepponen, J.J. Hakkarainen, I. De Meester, A.M. Lambeir, M. M. Forsberg, The effect of prolyl oligopeptidase inhibition on extracellular acetylcholine and dopamine levels in the rat striatum, Neurochem. Int 60 (2012) 301–309.
[53] M.M. Savitski, F.B. Reinhard, H. Franken, T. Werner, M.F. Savitski, D. Eberhard, D. Martinez Molina, R. Jafari, R.B. Dovega, S. Klaeger, B. Kuster, P. Nordlund, M. Bantscheff, G. Drewes, Tracking cancer drugs in living cells by thermal profiling of the proteome, Science 346 (2014), 1255784.
[54] H. Franken, T. Mathieson, D. Childs, G.M. Sweetman, T. Werner, I. Tögel, C. Doce, S. Gade, M. Bantscheff, G. Drewes, F.B. Reinhard, W. Huber, M.M. Savitski, Thermal proteome profiling for unbiased identification of direct and indirect drug targets using multiplexed quantitative mass spectrometry, Nat. Protoc. 10 (2015) 1567–1593.
[55] A. Mateus, T.A. Maatta, M.M. Savitski, Thermal proteome profiling: unbiased assessment of protein state through heat-induced stability changes, Proteome Sci. 15 (2017) 13, 017-0122-4. eCollection 2016.
[56] E.M. Del Amo, A.K. Rimpela, E. Heikkinen, O.K. Kari, E. Ramsay, T. Lajunen, et al., Pharmacokinetic aspects of retinal drug delivery, Prog. Retin. Eye Res. (2016).